Discrimination between Functional and Non-functional Cellular Gag Complexes involved in HIV-1 Assembly

Yisong Deng [1‡], John A. Hammond [1‡], Raymond Pauszek [1], Stosh Ozog [2], Ilean Chai [2], Jessica Rabuck-Gibbons [1], Rajan Lamichhane [1†], Scott C. Henderson [3], David P. Millar [1], Bruce E. Torbett [2] and James R. Williamson [1,4,5*§]

*1 - **Department of Integrative Structural and Computational Biology,** The Scripps Research Institute, La Jolla, CA 92037, United States*
*2 - **Department of Immunology and Microbiology,** The Scripps Research Institute, La Jolla, CA 92037, United States*
*3 - **Department of Molecular Medicine,** The Scripps Research Institute, La Jolla, CA 92037, United States*
*4 - **Department of Chemistry,** The Scripps Research Institute, La Jolla, CA 92037, United States*
*5 - **The Skaggs Institute of Chemical Biology,** The Scripps Research Institute, La Jolla, CA 92037, United States*

***Correspondence to James R. Williamson:** jrwill@scripps.edu (J.R. Williamson)*
https://doi.org/10.1016/j.jmb.2021.166842
Edited by Eric O. Freed

Abstract

HIV-1 Gag and Gag-Pol are responsible for viral assembly and maturation and represent a major paradigm for enveloped virus assembly. Numerous intracellular Gag-containing complexes (GCCs) have been identified in cellular lysates using sucrose gradient ultracentrifugation. While these complexes are universally present in Gag-expressing cells, their roles in virus assembly are not well understood. Here we demonstrate that most GCC species are predominantly comprised of monomeric or dimeric Gag molecules bound to ribosomal complexes, and as such, are not on-pathway intermediates in HIV assembly. Rather, these GCCs represent a population of Gag that is not yet functionally committed for incorporation into a viable virion precursor. We hypothesize that these complexes act as a reservoir of monomeric Gag that can incorporate into assembling viruses, and serve to mitigate non-specific intracellular Gag oligomerization. We have identified a subset of large GCC complexes, comprising more than 20 Gag molecules, that may be equivalent to membrane-associated puncta previously shown to be *bona fide* assembling-virus intermediates. This work provides a clear rationale for the existence of diverse GCCs, and serves as the foundation for characterizing on-pathway intermediates early in virus assembly.

Introduction

HIV-1 Gag and Gag-Pol are multifunctional polyproteins responsible for viral assembly, release, and maturation. The most abundant structural isoform Gag is comprised of matrix (MA), capsid (CA), nucleocapsid (NC), P6, P2, and P1 subdomains.[1] Virus and virus-like particle (VLP) assembly is thought to begin by binding of Gag's NC domain to the HIV RNA genome's Psi (Ψ) element.[2–7] This leads to three pivotal events: dimerization of Gag on the Ψ element nucleated by the NC domain and stabilized by the CA and SP1 domains, dimerization of the HIV-1 genome through extended base pairing of the 5′ UTRs, and localization of Gag to the plasma membrane via the MA domain,[6,8–15] with the temporal order of these events unclear. Assembly then proceeds through incorporation of other Gag, Gag-Pol, and Env gene products. During this Gag oligomerization process, multiple CA-SP1 regions lock into a 6-helix bundle structure to ensure proper Gag lattice forma-

tion.[11,12] Eventually, fully assembled virions and VLPs leave the cell through P6 domain-mediated budding.[16–19]

Assembly of Gag into an immature (pre-proteolyzed) form has been studied using a variety of cellular and *in vitro* techniques.[15,20–25] Intriguingly, purified Gag and non-specific RNA or DNA molecules are all that are required for spontaneous formation of spherical virus-like particles (VLPs) *in vitro*, while off-membrane VLP formation is inhibited in the cytoplasm of bacterial and human cells.[26–28] The mechanistic basis for cytoplasmic inhibition of Gag oligomerization in the absence of membrane binding has not been established.

Because Gag assembly is a multi-step process, it is not surprising to find several Gag-containing complexes (GCCs) that can be isolated from cells and separated via sucrose gradient sedimentation.[23,25,29–35] Most of these GCCs are formed in all human cell types tested, as well as in wheat germ extracts.[23,29] These GCC populations, named for their relative sedimentation coefficients as 10S, 80S, 150S, 500S and 750S, have been proposed to be stepwise intermediates for HIV assembly.[35,36] Smaller GCCs have been suggested to play integral functions in the earliest steps of HIV assembly, being composed of both cellular and viral factors, while larger complexes are thought to represent later, mainly viral, assembly products.[22,29,34,35] However, the exact makeup, functions and fates of these GCCs are still unclear.

In this work we both expand on the characterization of the biophysical properties and biomolecular makeup of GCCs produced during Gag expression in cells as well as identify several previously uncharacterized GCC species. Further, we demonstrate that the largest GCCs are not a single species, but rather a collection of many-sized GCCs whose mass largely reflects their Gag oligomerization state, while smaller GCCs are almost exclusively comprised of complexes that contain only 1 or 2 Gag molecules. We demonstrate that some of these species are not oligomeric Gag in the process of assembly, but rather monomeric and dimeric Gag associated with various ribosomal particles. Finally, using isotopic pulse labelling of cells combined with mass spectroscopy, we demonstrate that the smaller GCCs represent a highly dynamic Gag population that can be incorporated into assembling HIV particles, and that the largest GCCs exhibit labeling kinetics consisting with on-pathway production of VLPs. This data together implies at least two major Gag-binding pathways in the cell; a viral assembly pathway that reflects previous assembly studies lacking multiple kinetically-paused assembly intermediates,[1,8,22] and another pathway reflecting ribosome binding. We propose and discuss a model wherein ribosome-bound Gag can act as a reservoir of oligomerization-inhibited monomeric Gag ready to be incorporated into assembling particles at the membrane.

Results

GCCs are ubiquitous features of Gag expression in human cells

Previous studies have established ultracentrifugation as a reliable method for separating GCCs based on their relative molecular size.[29,32,37] To establish a GCC expression and purification system, HEK293T cells expressing Gag were lysed in a native lysis buffer (see materials and methods), and GCCs separated using a 10–80% step sucrose gradient (Figure 1(A)). Several distinct species were observed, with GCC boundaries mapping closely to the sucrose concentration borders. The slowest migrating species was previously named 10S, and 80S species identified as comigrating with the 80S ribosomal fraction.[29] The largest two peaks correspond to the 150S and 500S GCCs, respectively. Additionally, we observed a GCC population located between the 10S and 80S GCCs. A review of the literature revealed that indeed, this species was present in previous studies, but was not explicitly named or differentiated from the 80S GCC.[23,35,38,39] To address the concern that GCC separation was a possible artifact of the step-gradient where a continuum of complexes sedimented at the gradient boundaries, Gag lysates were sedimented using a 10–60% linear sucrose gradient with ultracentrifugation (Figure 1(B)). Each GCC observed in the step gradient was also observed in the linear gradient, including the previously uncharacterized population between 10S and 80S.

In the following work, we have discontinued the use of S values to identify each GCC, for two reasons. First, since the unnamed GCC between 10S and 80S has an unknown S value, and second, the 500S could be at sedimentation equilibrium rather than undergoing steady state sedimentation velocity (see below) (Figure 2(B)). Therefore, a less specific nomenclature system was adopted. Here, the first GCC species is labeled α, followed by β, γ, δ, and ε (Figure 1(B)). Lysates containing Gag with a super-folder GFP (sfGFP) inserted between the MA and CA domains (Gag-isfGFP), as well as Gag expressed in a full-length viral context, resulted in the production of the entire set of GCCs (Figure 1(B), for a full list of constructs used in this study see Supplementary Figure 1(A)), indicating GCC production is independent of the genetic context and only requires the production of full-length Gag. Further, GCCs are present when low levels of Gag are expressed from HEK293 and Jurkat cells containing a Dox-regulated integrated NL4-3 provirus (Figure 1(C)).[40,41] Our observations, together with extensive previously published data,[23,29,32–39,42–47] imply that the presence of

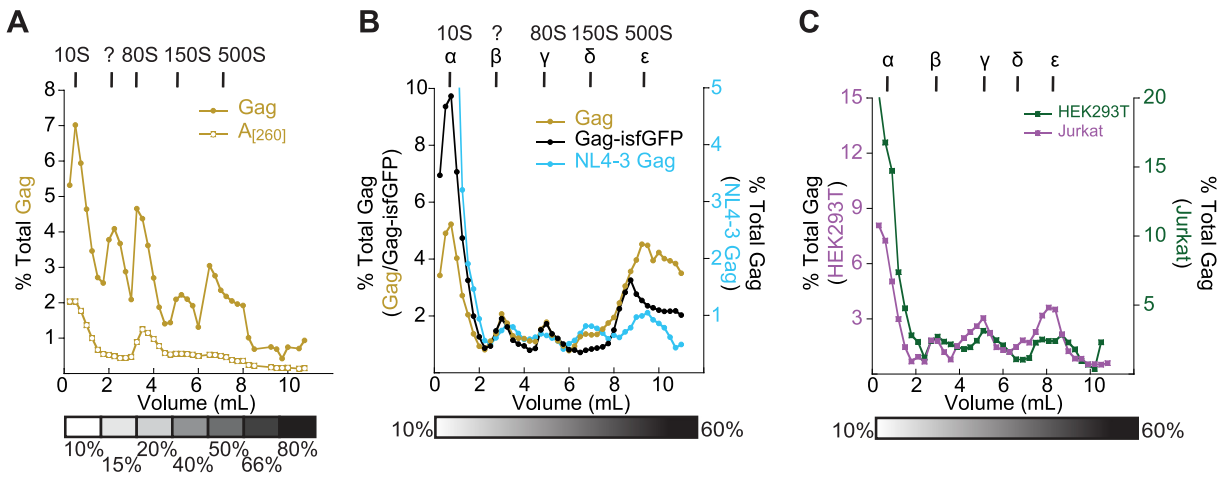

Figure 1. GCC distribution in sucrose gradients. (A) 10–80% step sucrose gradient. Gag distribution in filled circles and $A_{[260]}$ in open circles. (B) 10–60% linear sucrose gradient. Distribution of GCCs due to transfection of three different plasmids, WT Gag (brown), Gag-isfGFP (black), and pNL4-3 (blue). (C) 10–60% linear sucrose gradient. Distribution of GCCs resulting from proviral HIV in HEK293T (purple) and Jurkat (green) strains. For all panels, GCC naming scheme annotated on top and diagram of sucrose concentration on bottom.

GCCs are a universal feature of Gag expression in various mammalian cell types.

GCCs are more numerous than previously reported

Previous studies have reported conflicting results regarding assembly fidelity of Gag constructs containing a fluorescent protein between the MA and CA domains (annotated as internal by an "i" in the construct name, as in Gag-isfGFP).[48,49] For example, one study indicated such an insertion led to a reduction in virus accumulation extracellularly.[50] However, we found that these constructs efficiently produced VLPs (data not shown) with similar morphologies to WT Gag as verified by negative stain electron microscopy (Supplementary Figure 1(B)) as well as show a GCC distribution in sucrose gradients similar to WT Gag. Like all viral domain constructs used in this study, pGag-isfGFP-CTE contains an intact Ψ element in its 5′ untranslated region. This construct produces all GCCs seen in WT Gag and proviral constructs (Figure 1(B) and (C)). We therefore used the pGag-isfGFP-CTE plasmid as a model Gag expression platform for further biophysical characterization.

There is a strong possibility that any GCC can be composed of multiple indistinguishable species due to the overlapping nature of broad peaks in a sucrose gradient exacerbated by hand-fractionation, as well as the presence of a high-percentage sucrose cushion at the bottom of the gradient where many cellular species accumulate. Monitoring Gag during continuous elution of the gradient using both fluorescence and UV absorbance, revealed two distinct Gag species that were present within the γ population (named γ_1 and γ_2) (Supplementary Figure 2(A)). The γ_1 and γ_2 components were also observed using hand fractionation and modification of the sucrose gradient and centrifugation conditions to better resolve smaller GCCs (Figure 2(A)). Importantly, both of these peaks also exhibited a strong absorbance at 260 nm. It is well known that the small subunit (40S), large subunit (60S), and complete ribosome (80S) complexes migrate as discrete species when subjected to sucrose gradient ultracentrifugation.[51] Coincident Gag and $A_{[260]}$ signals indicate that GCCs β, γ_1, and γ_2 migrate in a pattern that is very similar to the 40S, 60S and 80S ribosomal peaks.

The largest GCC (ε) was also comprised of multiple species (Figure 2(B)). Previous reports established GCC nomenclature based on their apparent sedimentation rates in sucrose gradients.[29,37] The S values can only be determined when a particle is undergoing constant velocity sedimentation (when the sedimentation rate is greater than the rate of diffusion).[52,53] However, with high sucrose concentrations, the rates of diffusion of many molecules equal the rates of sedimentation, thus coming to an equilibrium. In this case, the position in the gradient does not reflect an S value that correlates with the size and shape of the particle.[54] When a time course of ultracentrifugation was performed, a distinct high-molecular-weight species was observed that quickly came to sedimentation equilibrium within high sucrose-containing aliquots (referred to as a sucrose cushion) (Figure 2(B)). The signal then increased over time as subsequent smaller GCCs begin accumulating at the sucrose cushion. Therefore, population ε is likely comprised of many GCCs of increasing sedimentation rates that cannot be distinguished individually using these methods.

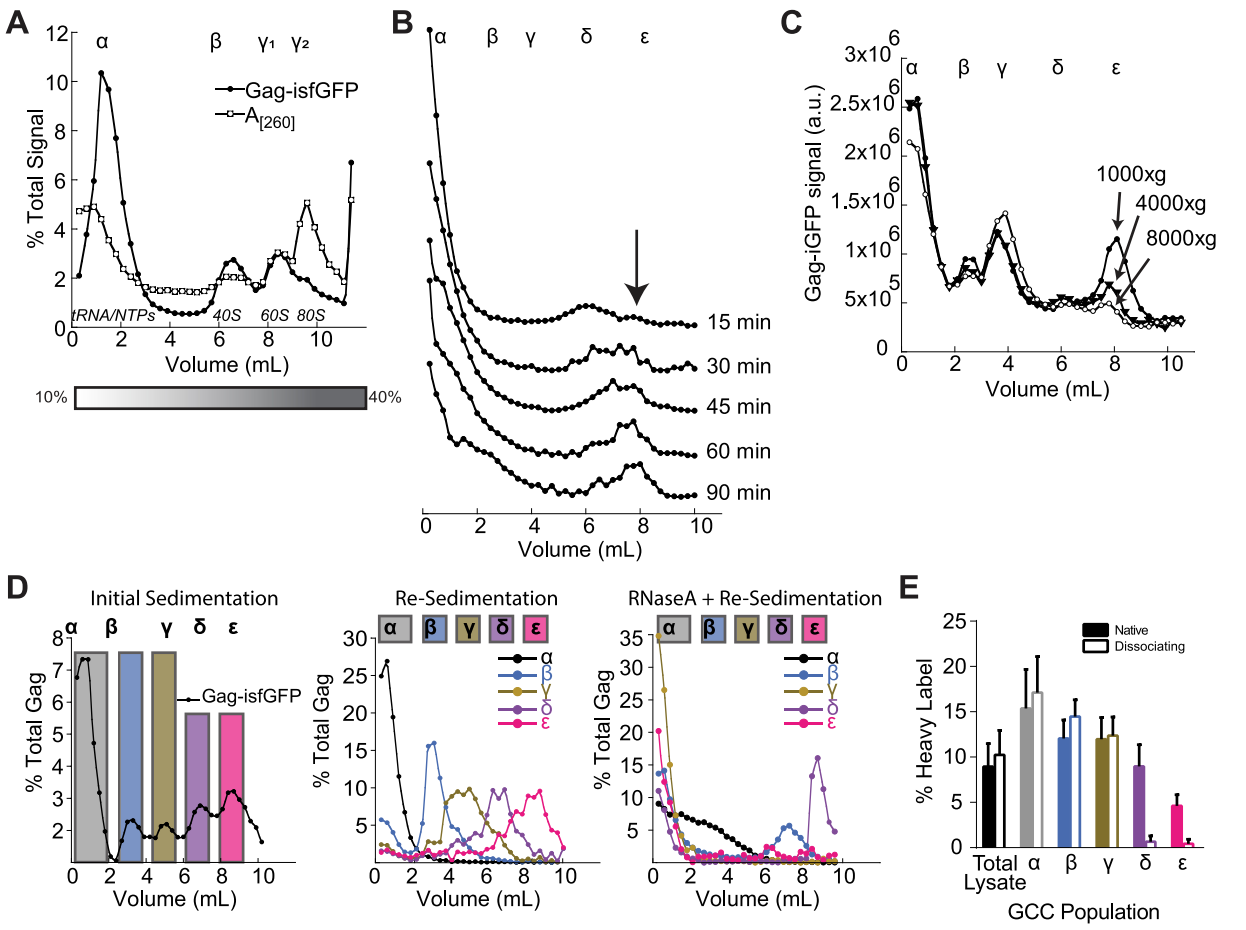

Figure 2. Biophysical Characterization of GCCs in sucrose gradient. (A) Gag distribution in 10–40% sucrose gradient. Gag-isfGFP distribution in filled circles, and $A_{[260]}$ in open. Population designations above graph, and sucrose concentration diagram below. Major cellular RNA population resulting in $A_{[260]}$ signal are noted under curves. (B) GCC distribution in 10–60% sucrose gradient using a variety of ultracentrifugation times (listed to right of each run). Names on top denote projected migration location of each GCC species when run for a standard 3 h. Arrow indicates final migration spot for ε species. (C) The effects of lysate clearing centrifugation speed on GCC distribution. 10–60% gradient was used, and GCC population names listed above graph. (D) GCC stability assays. GCC populations were individually pooled and buffer exchanged (left panel), and resedimented on separate sucrose gradients in the absence (middle panel) or presence of RNase A. Colored boxes represent GCC pooled fractions, and colors represent each GCC. Location of expected GCC migration is marked at top of each graph. (E) Gag spike assay. The distribution of exogenously produced heavy-labelled Gag in Gag-expressing lysate fractions. X axis denotes pooled GCC fractions. Solid bars are under native conditions, and open bars are under ribosome dissociating conditions.

The largest GCC, ε, is sensitive to the nuclear-clearing step of lysate preparation (Figure 2(C)). A typical nuclear clearing procedure involves the use of a centrifugation step at or above 8000*g* for 10 min prior to ultracentrifugation. However, this will also clear large GCCs from solution. As this centrifugal force was lowered, the overall ε population signal increased. This finding is consistent with previous reports which indicate this population is comprised primarily of large assembling viral and viral-like particles.[33–35] Therefore, there are many previously unidentified GCC species located throughout the gradient, with the high-molecular-weight ε population being particularly numerous and highly susceptible to sedimentation pelleting.

GCCs are stable but RNase sensitive

The many GCC species that make up the ε population may be a byproduct of GCC disassembly during centrifugation. To evaluate this possibility, GCC stability was assessed by crosslinking lysates and assaying for changes in Gag distribution post ultracentrifugation (Supplementary Figure 2(C)). Several crosslinker concentrations were successful in efficiently binding GCC molecules together but resulted in

no discernable changes in GCC distribution, indicating that intermediately sized GCCs are not likely dissociated Gag complexes.

While these complexes do not disassemble during centrifugation, it is possible they dissociate after they are purified from the sucrose. To assess their cohesive stability post-centrifugation, GCCs were purified (Figure 2(D), left panel), allowed to remain for a day at 4 °C, and re-sedimented on separate sucrose gradients (Figure 2(D), middle panel). All GCCs migrated to expected positions within the sucrose gradient, with only a small fraction disassembling into smaller GCCs. Therefore, the integrity of GCCs can be maintained during and after sedimentation for biophysical characterization.

Previous work identified the γ population as containing the first functional Gag/genome interaction.[34] This report also suggested RNA as the molecule responsible for the increase in complex mass.[34,38] This was verified when all purified GCCs were subsequently incubated with RNase A prior to re-sedimentation (Figure 2(D), right panel). Every GCC experienced a change in their sucrose gradient migration during ultracentrifugation, with most Gag now localized to the top of the gradient, due to a decrease in molecular mass. However, some GCCs migrated further into the gradient, indicating an increase in molecular mass. The cause for this effect is unclear but may be due to an increase in Gag oligomerization nucleated via incompletely digested RNA (see discussion). These results indicate that all GCCs require RNA for their stable localization within the sucrose gradient.

Gag exchange between GCCs is dynamic post-lysis

While GCCs are stable post-centrifugation, Gag's exchange between complexes during the lysis step is not well understood. To better understand the dynamic interchange between GCCs, we assessed the incorporation efficiency of exogenously produced Gag into cellularly-produced GCCs. First, the α population from isotopically labeled Gag produced in SILAC (Stable Isotope Labeling by/with Amino acids in Cell culture) HEK293T cells was purified. This was then added to unlabeled Gag-expressing cells in native lysis buffer. This mixture was processed by sucrose gradient ultracentrifugation as above, and the ratio of labeled vs. unlabeled Gag in each GCC species quantified using mass spectrometry (Figure 2(E)). In the final lysate, exogenously produced Gag comprised 8.8% of the total Gag found. If Gag does not exchange between GCCs once cells are lysed, then the exogenous Gag should be localized to the α population only. Indeed, the α population contained the highest percentage of isotopically labeled Gag at 15.2%. However, Gag located in β, γ, δ, and ε populations were also labelled at 12.0%, 11.9%, 9.2%, and 4.6% respectively. These results indicate that all GCCs can incorporate exogenous Gag, though this incorporation occurs less frequently as the GCCs increase in size. Moreover, this suggests Gag can move between complexes post lysis, and such movement is inhibited once GCCs are isolated.

GCCs exhibit a mixed oligomerization profile

Previous models have proposed that GCC α contains Gag in a low oligomerization state and further imply Gag oligomerization increases as GCC size increases.[34–36] If the GCC γ particle was entirely composed of Gag, one might expect on the order of ~60 monomers in the complex to achieve the 3 MDa size of the 80S ribosome. However, GCCs are likely also comprised of RNA molecules (Figure 2(D)), making determination of Gag oligomerization solely based on molecular weight difficult. Single-molecule total internal reflection fluorescence (smTIRF) microscopy was used to quantify the oligomerization state of Gag in each GCC directly. Individual GCCs containing a Gag-isfGFP fusion construct (Supplementary Figure 1(A)) from diluted sucrose gradient fractions were captured on the surface of a quartz microscope slide via immobilized α-GFP antibodies (Figure 3(A)) and imaged as discrete fluorescent spots within the field of view. Under these conditions, the fluorescence intensity of each spot was proportional to the number of sfGFP (Gag) molecules contained in the complex (Figure 3(B)).

Due to the large range of expected fluorescence intensity of highly oligomeric complexes across different gradient fractions, monomer counting by photobleaching is not feasible. Instead, as a control, we also carried out an experiment using bacterially expressed and purified sfGFP (see Supplementary Figure 1(A) for construct description) to determine the average fluorescence intensity of a single monomer. A histogram of the average initial intensity of many individual spots exhibits an approximately gaussian distribution with a small shoulder at the high intensity edge (Supplementary Figure 3(A)). The histogram is adequately described by a linear combination of two gaussian distributions with mean μ_0 and $2\mu_0$ and a shared variance. This result indicates that sfGFP exists primarily as a monomer with a mean fluorescence intensity of 190 ± 90 a.u., along with a small dimer population. One caveat for these measurements is that complexes containing more than ~40 Gag monomers will have an intensity that exceeds the dynamic range of the instrument, and therefore in these cases the calculated count represents a lower limit on the number of Gags present.

GCC populations α, β, and γ were comprised almost exclusively of low oligomerization state Gag-isfGFP (monomer and dimer) (Figure 3(D) and Supplementary Figure 3(B)), with the

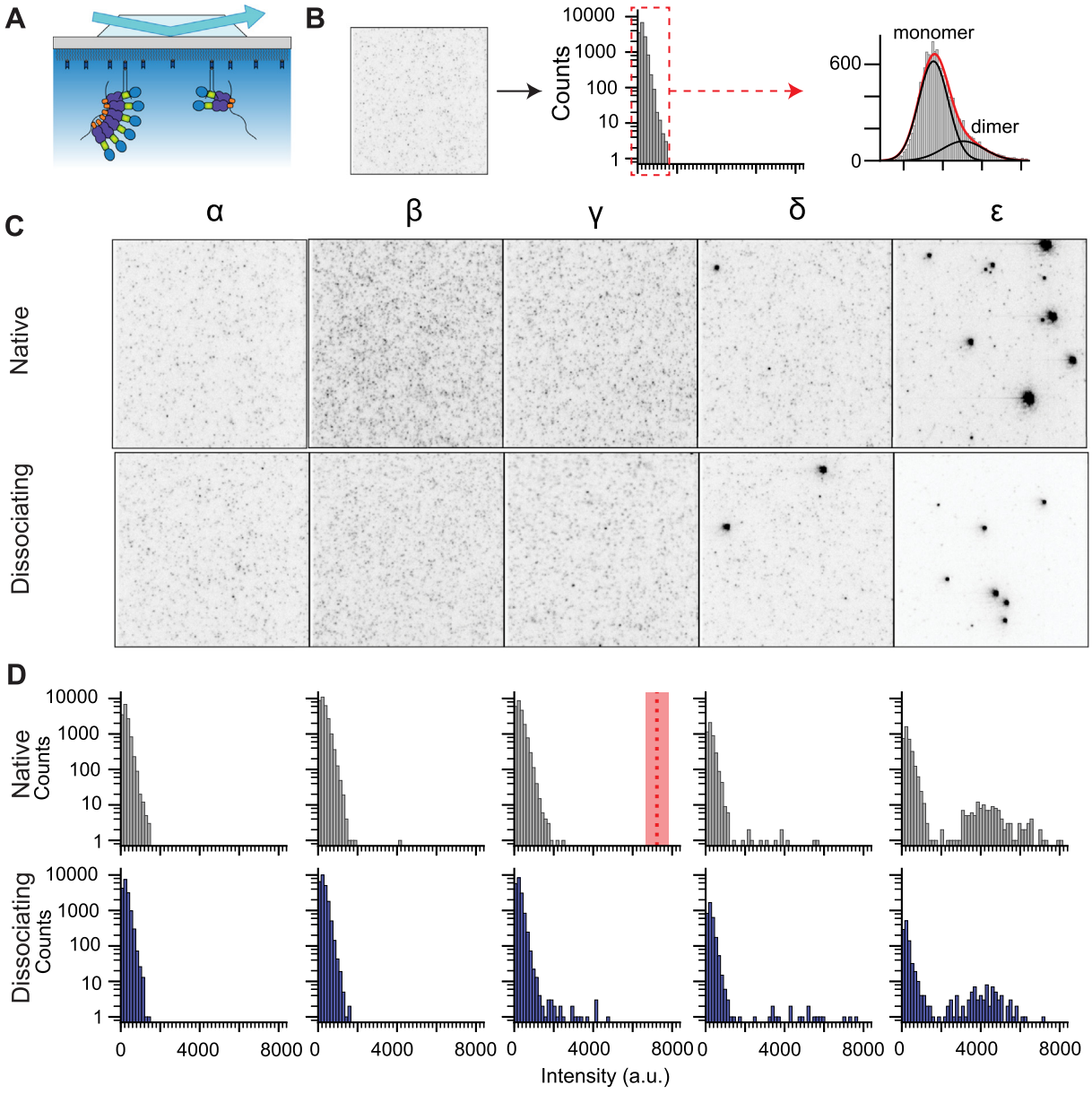

Figure 3. Gag oligomerization in each GCC. (A) Schematic representation of TIRF experiment. Gag-isfGFP is immobilized on a quartz surface via an α-GFP antibody. An evanescent fluorescent field is created using total internal reflection of a 488 nm laser at the quartz surface. (B) A representative TIRF image for GCC α in left panel, the resulting histogram for all data on log scale in middle panel, and re-graphed low-intensity data on a linear scale with monomer and dimer species modelled in black and labelled on top within right panel. Red line in right panel represents resulting fit from monomer and dimer gaussian fits, and best describes all low intensity data. (C) Representative TIRF images for each GCC species, under both native (top row) and dissociating (bottom row) lysis conditions. (D) Intensity histograms for each GCC using accumulated intensity data. Lower intensities indicate lower oligomerization states of Gag. See Supplementary Figure 3(B) for higher magnification and re-graphing using a linear scale of low intensity distributions.

population intensity distributions closely resembling that of purified sfGFP (Supplementary Figure 3(A)). The δ population exhibited some complexes that contain up to ~20 Gag-sfGFP monomers (up to ~4000 a.u., Figure 3(D)) while population ε contains complexes in a range of oligomerization states up to the limit of detection for the assay. However, both later fractions also contained a significant number of low oligomerization state Gag species (Figure 3(D) and Supplementary Figure 3(B)). The proportion of low to high oligomerization state species in these fractions was surprising given the relative sizes of each of the GCCs (Supplementary Figure 3(C)). It is

possible highly oligomerized GCCs are immobilized less efficiently than Gag monomers and dimers. The presence of large Gag oligomers in the δ and ε fractions indicate that immobilization is possible, though the relative immobilization efficiency cannot be determined. Under conditions where the antibody binding is saturated, these differences in binding efficiency would result in a skewed oligomerization profile. To control for concentration-dependent effects of binding, multiple dilutions of all samples were tested for the presence of oligomerized Gag Species (data not shown). No highly oligomerized species were discovered in the α or β GCC populations under any dilution condition, and only a few low-level oligomerization events in the γ population. Further, the ratios of high vs. low oligomerization did not change substantially for any dilution tested (data not shown). While some of the low oligomerization state GCCs in δ and ε fractions might be explained by Gag molecules dissociating from highly oligomerized Gag, our previous data indicates that these complexes are very stable and do not significantly dissociate during or after centrifugation (Figure 2(D), Supplementary Figure 2(C)). Therefore, these data suggest that the majority of GCCs in these later fractions are composed primarily, by mass, of some other (unlabeled) cellular components bound to one or two Gag molecules.

To test this hypothesis, functional Gag mutants were assayed for their GCC production and distribution. Mutations that affect the subcellular distribution (and hence the oligomerization state) of Gag would still present as large molecular weight Gag, if Gag is indeed associated with large cellular complexes. Three classes of Gag mutations were tested: G2A is a mutation that prevents myristoylation, and hence Gag association with the membrane and subsequent oligomerization and assembly,[55] EE207/208AA affects Gag assembly and its ability to create curvature at the cell membrane, but does not affect subcellular localization,[56–58] ΔNC and HH400/421CC both affect Gag's ability to bind RNA, affecting its subsequent oligomerization, but should not affect membrane binding (Figure 4(A)).[59,60]

While each mutation exhibits similar defects in producing extracellular VLPs, their intracellular localization and GCC distribution differs (Figure 4 (B)–(D)). Gag-isfGFP G2A is diffusely cytoplasmic and contains no puncta distinctive to highly oligomerized Gag. However, G2A clearly produces some δ and ε GCCs, though at a lower frequency than WT. A similar GCC distribution was again observed for EE207/208AA, though the cells show a different subcellular localization when imaged using confocal microscopy. The only mutations totally lacking the ability to create any larger molecular weight GCCs were ΔNC and HH400/421CC, which is not surprising given GCC instability in the presence of RNase A (Figure 2 (D)). Our results suggest there was no clear correlation between the subcellular localization of the Gag mutants and the production of larger GCCs. For example, a mutant (G2A) unable to associate with the membrane does not oligomerize in the cytoplasm, yet still forms large GCCs (albeit at a lower efficiency than WT). However, other mutants (ΔNC and HH401/402CC) which are defective in RNA binding still effectively associate with the cell's membrane but display no evidence of large GCC formation. All this data taken together strongly suggests that some Gag in a low oligomerization state is binding to large molecular weight complexes, and these complexes are coincident with assembling Gag in sucrose gradients.

Some GCCs are comprised of Gag bound to ribosomes

Monomeric Gag in the δ and ε populations could be binding to cellular complexes that have a wide variety of masses. These complexes must have an RNA component, which affords structural stability, and are abundant enough to accommodate many Gag molecules. Since GCCs β, γ1, and γ2 co-migrate with rRNAs (Figure 2(A), Supplementary Figure 2(A)), it is possible that Gag is directly interacting with ribosomal subunits. Indeed, all GCC positions within the sucrose gradient match tRNA and rRNA distributions closely (Figure 5(A) and (B)).

If Gag binds to ribosome complexes directly, then the distribution of GCCs should change when the ribosomal complex distribution is altered. Lysis buffer lacking magnesium will result in the dissociation of 80S ribosomes and polysomes into their cognate 40S and 60S subunits. Further, increasing the sodium concentration will cause the ribosomal subunits to migrate slower within the sucrose gradient (Figure 5(A) and (B)). These ribosomal dissociating conditions also resulted in notable similar changes in GCC distribution. It should be noted that all sodium and magnesium concentrations used in these studies are within accepted parameters for efficient association between Gag and the Ψ packaging RNA element *in vitro* and in cells.[35,37,59]

To test the ability of Gag to directly interact with ribosomes, purified bacterially expressed Gag with eGFP inserted between the MA and CA domains (named Gag-ieGFP) (Figure 5(C)) was incubated with purified 80S ribosomes, and again sedimented on a sucrose gradient (Figure 5(D)). Gag distribution mirrored expected ribosomal 40S, 60S and 80S distribution, in contrast to Gag alone which did not efficiently enter the gradient.

Polysome-bound Gag molecules migrate to the bottom half of the sucrose gradient. This effect may explain why some monomer and dimer Gag species are found there, as well as why

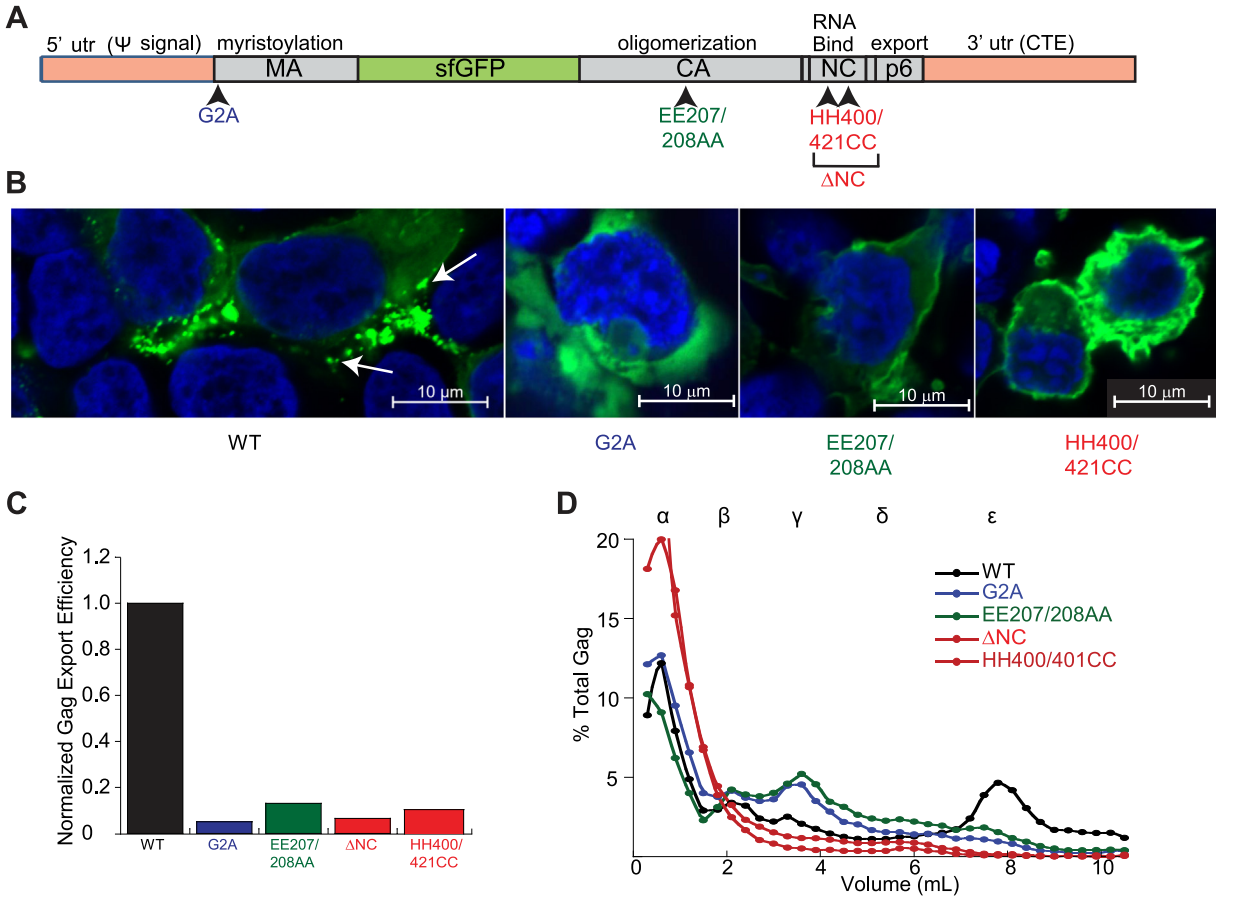

Figure 4. Gag mutants and GCC formation. (A) Diagram of Gag constructs used in these experiments. Functional effect of Gag domains listed at top, and mutations affecting that role listed on bottom. Numbering reflects mutation position at WT Gag gene with sfGFP absent. (B) Confocal images of HEK293T cells expressing (from left to right) WT, G2A, EE207/208AA, and HH400/421CC Gag-isfGFP. Gag signal in green, and nuclei stained in blue. Arrows denote "puncta" formation on membrane of cells. (C) Gag export efficiency into media. (D) Gag distribution in 10–60% sucrose gradient for each mutant. GCC position annotated above the graph.

exogenous Gag seems to incorporate into large GCCs (Figure 2(E)). To test this hypothesis, Gag oligomerization was again assessed for each GCC under ribosome dissociating conditions (Figure 3(C) and (D)). A marked decrease in monomeric and dimeric species was found in the ε population, leading to a significant change in its oligomerization ratio (Supplementary Figure 3(C)). We also retested the ability of exogenous Gag to incorporate into cellular GCCs during lysis under ribosome dissociating conditions. Here, exogenous Gag no longer efficiently incorporated into δ and ε GCCs (Figure 2(E)). These results, when taken together, strongly support the hypothesis that monomeric Gag is robustly yet transiently associating with ribosomal complexes to form GCCs of large molecular weight. Further, this data indicates almost all the β, γ1, γ2, complexes are ribosome associated, while comprising a smaller proportion of the ε population.

Ribosome-bound gag represents assembly start points, not intermediates

To better understand the role of ribosome binding during HIV assembly, isotopic pulse labeling experiments were performed. Here, isotope-labeled amino acids are introduced to the cell, and subsequently incorporated into nascently translated proteins, resulting in a labeling kinetic profile (Figure 6). The labeling kinetics for proteins in cells is determined by their beginning pool size, synthesis rate, and dissipation rate. In general, proteins with small initial pool sizes and fast synthesis and dissipation rates will label more quickly than those with large pool sizes and slow synthesis and dissipation rates. Gag-isfGFP-expressing HEK293T cells were grown in media containing ^{13}C labeled arginine and lysine and the rate of isotope incorporation in proteins assayed via mass spectrometry (Figure 6(A)). As expected, Gag incorporated the isotopic labels faster than

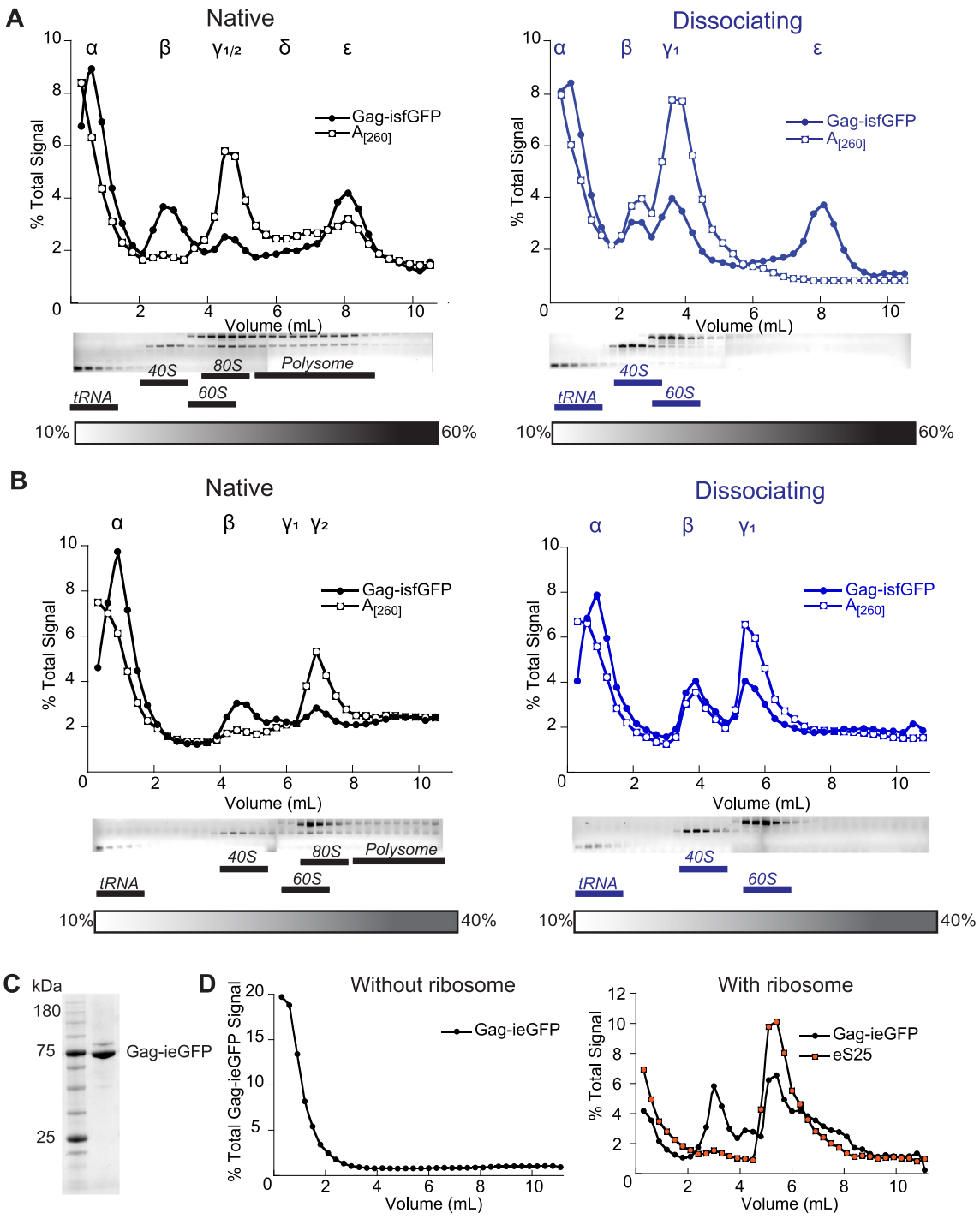

Figure 5. Gag distribution follows ribosome distribution. (A and B) Gag distribution under native (left and in black) and ribosome dissociating (right and in blue) conditions, using 10–60% sucrose gradient (A) or 10–40% sucrose gradient (B). In each case, Gag signal is represented by solid circles, and $A_{[260]}$ signal represented by open circles. Agarose gels of RNA from each aliquot are displayed below each graph, with major RNA species labelled in italics. GCC populations are designated atop graphs. (C) SDS PAGE gel of purified Gag-ieGFP. (D) Purified Gag-ieGFP (black circle) migration within a 10–60% sucrose gradient in the absence or presence of purified ribosomes (orange squares) whose eS25 subunit has been fluorescently labelled for quantification.

native cellular proteins (Figure 6(A)). This is likely due to a high synthesis rate of Gag, as well as a high dissipation rate (due to VLP production).

Previous work has implicated GCCs α, γ, δ, and ε as on-pathway and stepwise intermediates in an HIV assembly process.[29,35,36] The observation that

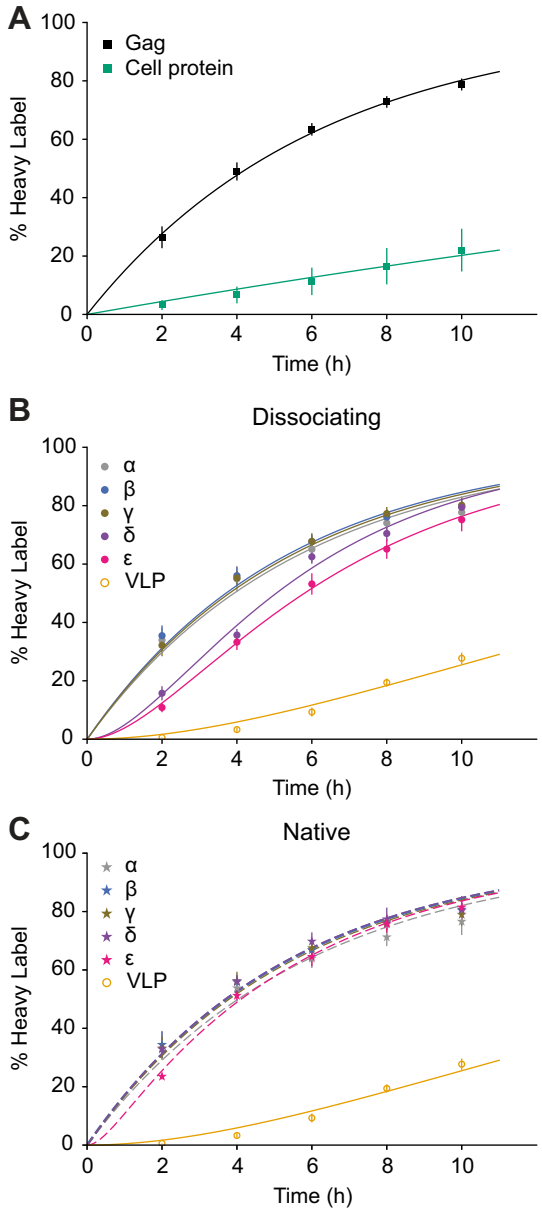

Figure 6. Role of GCCs during assembly revealed by Gag pulse labeling. (A) Quantification and fitting of isotopic labeling efficiency of Gag and representative cellular proteins from cleared cell lysate. Gag average quantification calculated from 7 different peptides. Cell proteins average quantification calculated from 8 different proteins. (B and C) Quantification and fitting of isotopic labeling efficiency of Gag from GCCs α, β, γ, δ, ε and VLP under ribosome dissociating condition (B) and native condition (C). Gag average quantification calculated from 7 different peptides.

these GCCs contain a significant amount of ribosome-bound Gag makes it unclear if they are true assembly intermediates. This same isotopic-labeling method can be used to assess the role of each GCCs in an assembly pathway. For example, in a linear assembly pathway, early intermediates would be expected to label at a faster rate than later intermediates, and all should label faster than the ending product. Under ribosome-dissociating conditions, GCCs α, β, and γ label at identical rates, in contrast to the δ, ε, and VLP populations, which demonstrate successive lags in their labeling curves (Figure 6(B)). Here, the pulse result is consistent with a model where GCCs α, β, and γ are either parallel or interchangeable first steps in the Gag assembly pathway, while GCCs δ and ε are later, on-pathway steps. As expected, VLPs showed the most significant lag in labeling kinetics, a hallmark of a pathway endpoint.

It is possible that a small number of on-pathway intermediates exist within the abundant ribosome-bound Gag populations β and γ. These intermediates should exhibit a labeling rate that is faster than ribosome-bound Gag, but slower than Gag in GCC γ. However, the presence of abundant ribosome-bound Gag can dominate the labeling result, as shown for GCCs β, γ, δ, and ε under native conditions (Figure 6(C)). Under ribosome-dissociating conditions, the differentiation of Gag assembly intermediates and ribosome-bound Gag can only be observed for GCCs δ and ε, because the labeling rate for GCCs β and γ is still dominated by ribosome-bound Gag (Figure 6(B)). The possibility exists that if Gag bound to ribosomes were to be depleted from GCCs β and γ, more pronounced labeling lags would result from on-pathway Gag species found in these fractions

Discussion

GCCs during assembly: Two overlapping processes

Cellular production of HIV-1 involves the assembly of multiple viral and cellular factors into a cohesive and infectious virion structure. This process is wholly dependent on virally encoded Gag, which binds to an RNA element Ψ located within the 5′ UTR of the viral genome and initiates assembly. Along with this initial binding, Gag and Ψ both undergo structural transitions to facilitate assembly into an immature viral particle.[61–64] While many steps during HIV-1 assembly have been well characterized, there remain unanswered questions, such as the location, order, and composition of the earliest Gag assembly steps. Previous work resulted in the hypothesis that GCCs could represent intermediates on a Gag assembly pathway, acting as processing bodies for some, or all, of these structural transitions or binding events.[34–36,42] However, live cell imaging does not show temporal lags in the later stages of Gag oligomerization that would be necessary for intermediates to form.[22] Furthermore, previous pulse labeling of cells producing Gag has failed to unambiguously demonstrate labeling lags between early GCCs, which would be indicative of stepwise assembly intermediates[29,44]. Lastly, the δ (150S)

population was missing in several reports[33,35,38], although the reasons for this are not clear.

We have attempted to better define the molecular composition and biophysical properties of Gag-containing complexes, as well as further elucidate their functional roles during HIV assembly. While we observed the formation of all previously described GCCs, we found that the distribution of GCCs were affected dramatically by different lysis buffer conditions. The findings presented here suggest a model wherein Gag transiently binds ribosomes via an NC-RNA interaction. This model is consistent with previously published GCC findings that resulted in different interpretations of GCC pathways.[36] We propose that these sucrose gradients contain two overlapping but primarily independent processes: HIV assembly and Gag/ribosome binding (Figure 7).

Gag interactions with ribosomes in cells, *in vitro,* and *in virio* have been described extensively.[65–70] Because of the large body of literature describing this interaction, this study did not repeat these efforts beyond validating the ability of Gag to interact with ribosomal forms *in vitro* (Figure 4(D)). However, the results reported here yield a few intriguing novel observations about this interaction. First, in our experiments, Gag preferentially associates with dissociated ribosomal subunits over fully assembled ribosomes (Figures 2(A) and 5). This preference may be due to a large RNA surface located at the 40S-60S interface that becomes exposed upon ribosomal dissociation.[71] Second, this NC/RNA ribosomal interaction differs from previously reported protein–protein interaction with RPL7.[65] Third, while Gag may be interacting with messenger RNAs as a way of associating with some ribosomes, the interaction with both the dissociated 40S and 60S subunits indicates an mRNA-free interaction as well (Figure 5). Fourth, stable ribosomal binding is wholly dependent on the NC domain of Gag and cannot be recapitulated by the RNA-binding activity of MA (Figure 4(D)). Fifth, Gag is exclusively associated with ribosomes in a low oligomerization state.

The ability of Gag to interact with ribosomes may explain previous results measuring the diffusion rate of Gag in cells.[72] Here, it was found that a significant amount of low-oligomerization state Gag would transition between slow-diffusion and fast-diffusion modalities, and this transition was wholly

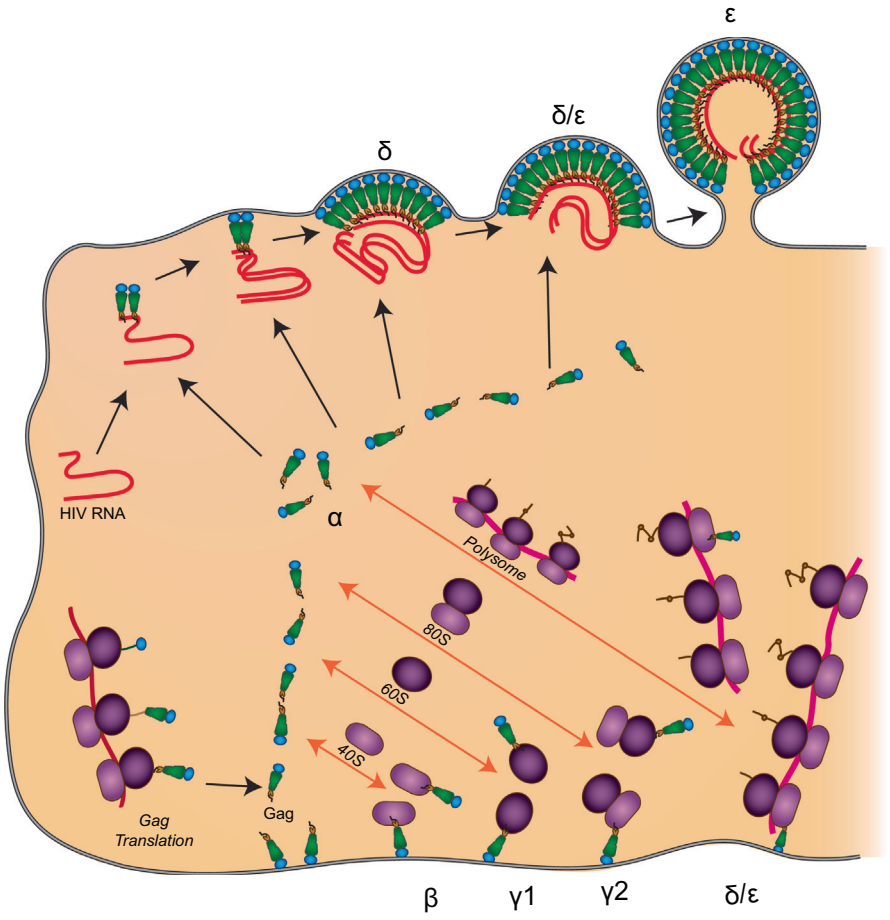

Figure 7. Model of GCC distribution and function in HIV assembly. Most Gag distribution on sucrose gradients represents two processes; HIV assembly, and Gag association with various tRNA and ribosomal complexes.

dependent on the NC domain. The large number of Gag molecules involved in this transition would argue against this being the first Gag/Ψ binding event. However, this is consistent with Gag binding transiently with ribosome species in the cytoplasm.

We believe the work here indicates that previously described early assembly intermediates[35] would represent a small fraction of the Gag found in the cell, and likely migrate within a sucrose gradient to locations dominated by ribosome-bound Gag.

A model for ribosome-mediated inhibition of Gag oligomerization and HIV assembly

While this study provides some evidence for Gag binding to ribosomes, we still do not understand the functional role, if any, of the Gag-ribosome interaction in the cell. It is possible this is a non-specific interaction that is of no relevance to viral assembly. However, previous work has established a functional role for Gag association with ribosomes, or with bodies that regulate ribosomal processes.[65,73,74] Beside these published roles, it is intriguing to note the effect on Gag migration within sucrose gradients upon the addition of RNAses (Figure 2(D)). When RNAs like tRNA or ribosomes are degraded by RNAse A, Gag begins to form larger complexes post-lysis. One possible interpretation would be that Gag is beginning to oligomerize around more-scarce large or incompletely digested RNAs. Gag readily oligomerizes around any available nucleic acid *in vitro* if the stoichiometric ratio of Gag is in far excess.[21,27] However, Gag oligomerization is actively inhibited in the cell's cytoplasm without binding to the membrane. Even when cytoplasmic Gag concentrations are increased via production of mutant protein (Gag G2A) which does not inhibit *in vitro* assembly, no oligomerized Gag is found (Figure 4(B) and Supplementary Figure 4). Further, unmyristoylated wild-type Gag produced in *E. coli* does not oligomerize intracellularly, even though it is expressed at vastly higher levels than is achieved in transfected mammalian cells.[21,27] This would indicate an inherent mechanism to inhibit Gag oligomerization in the cytoplasm. Models for assembly inhibition have been suggested previously. For example, Gag assembly is tightly regulated by the MA domain, requiring localization to the plasma membrane for efficient oligomerization around an RNA element.[75–77] These studies indicate tRNA binds to the MA domain, acting as an important quality control measure to inhibit premature Gag oligomerization in the cell. However, this model does not explain how NC-mediated oligomerization is inhibited pre-assembly. We hypothesize this mechanism involves the use of abundant RNAs in the cell acting as binding partners for Gag, actively inhibiting cytoplasmic oligomerization in concert with the RNA. Effectively, the ribosomes provide a convenient reservoir for monomeric Gag, allowing the specific initiation complexes to form involving Ψ and the membrane, without the potential interference of inappropriately oligomerized Gag complexes.

Under normal infection conditions, Gag represents a small amount of the total proteome of the cell. Even when Gag is expressed using transient transfection, its presence is difficult to detect using regular shotgun proteomics (data not shown). In contrast, ribosomes and tRNA represent the most abundant RNAs in the cell's cytoplasm. They are expressed in far excess of all HIV viral proteins by mass. It is possible ribosomes act as "sponges", transiently binding Gag in low-oligomerization states. Gag's NC domain prefers to bind single-stranded RNA regions, and ribosomes have few of these moieties on their surface, making oligomerization more difficult. These complexes would then act as Gag repositories. Here Gag would transiently dissociate and rebind abundant ribosomes in the cytoplasm. However, when not bound to ribosomes, Gag would be free to be incorporated into assembling virions at the cell membrane.

The study of Gag containing complexes presented in this study begins to define the roles of specific GCC species in HIV assembly during the viral lifecycle. Our results indicate that there are two major GCC binding pathways (Figure 7). One pathway includes GCCs with highly oligomerized Gag that have already entered the on-membrane assembly, consistent with previous studies showing a continuous assembly pathway lacking multiple kinetic pauses.[1,22,24] The second class represents monomeric or dimeric Gag associated with large abundant cellular RNAs, located in the cytosol prior to on-membrane assembly. We believe the formation of these latter Gag-cellular RNA complexes may represent an unappreciated aspect of virion assembly, serving as a reservoir of Gag to support the membrane assembly process as well as restricting off-membrane assembly. The ribosome-associated pool of Gag is abundant and dynamic, both preventing the formation of dysfunctional cytoplasmic viral aggregates and providing a supply of monomeric Gag for membrane-binding and oligomeric assembly. Taken together, these findings further clarify the roles of GCCs in the Gag assembly process and highlight the potential importance of Gag/cellular-RNA interactions as a pre-assembly step. While the late stages of Gag assembly, budding, and maturation have been well characterized, the details of the early steps for nucleation of Gag at the membrane with genomic RNA remain to be elucidated. This work provides key information about which GCCs should be focused on as functional on-pathway complexes that likely bridge the early and late stages of virion assembly.

Materials and Methods

Cells lines

HEK293-CD4-tetHIV-WT and Jurkat-tetHIV-WT cell lines were a kind gift from Dr. Mary Lewinski (University of California, San Diego) and have been described previously.[40,41] RPS25-SNAP-HAP1 cell lines were a kind gift from Dr. Joseph D. Puglisi (Stanford University School of Medicine, Stanford), HEK293T cells were purchased from ATCC.

HEK293-CD4-tetHIV-WT cells were cultured in DMEM supplemented with 10% tet-free FBS (Omega Scientific), 1x penicillin/streptomycin, 2 mM L-glutamine, 200 μg/mL G418 (Gibco), 200 μg/mL Zeocin and 200 μg/mL Puromycin.

Jurkat-tetHIV-WT cells were cultured in RPMI-1640 supplemented with 10% tet-free FBS (Omega Scientific), 1x penicillin/streptomycin, 2 mM L-glutamine, 200 μg/mL G418 and 1 μg/mL Puromycin.

RPS25-SNAP-HAP1 cells were cultured in IMDM supplemented with 10% FBS, 1x penicillin/streptomycin, 2 mM L-glutamine.

HEK293T cells were cultured in DMEM supplemented with 10% FBS, 1x penicillin/streptomycin, 2 mM L-glutamine.

SILAC adapted HEK293T cells were generated by culture regular HEK293T cells in SILAC DMEM (Thermo Scientific) supplemented with 10% dialyzed FBS (Gibco), 1x penicillin/Streptomycin, 2 mM L-glutamine, 0.798 mM regular L-Lysine and 0.398 mM regular L-Arginine for 2 generations.[78]

SILAC labeled HEK293T cells were generated by culture SILAC adapted HEK293T cells in SILAC DMEM (Thermo Scientific) supplemented with 10% dialyzed FBS (Gibco), 1x penicillin/Streptomycin, 2 mM L-glutamine, 0.798 mM 13C6 L-Lysine (Cambridge isotope laboratories inc.) and 0.398 mM 13C6 L-Arginine (Cambridge isotope laboratories inc.) for 5 generations.

Plasmids

pJL1-sfGFP was a generous gift of the Jewett lab. pGag-CTE-BH10 and pNL4-3 are described previously[79,80] (Genebank codes AH002345.2 and AF324493.2 respectively for HIV sequence information). pGag-CTE was created using the HiFi Gibson Cloning kit (NEB),[81] where the 5′ UTR and Gag coding region of BH10 strain were replaced by analogous NL4-3 elements ending at the P6 element. Subsequently, sfGFP[82] was inserted between the MA and CA domains, flanked by identical protease cleavage sites, as previously described[49] to create pGag-isfGFP-CTE. Finally, all point and deletion mutations were created using Q5 site-directed mutagenesis kit (NEB). pHis-Gag-EGFP-Δp6 was created using the HiFi Gibson Cloning kit (NEB),[81] where the gene encoding EGFP was inserted into the middle of the protease cleavage site between the MA and CA domains. Its parental plasmid pHis-GagΔp6 was a generous gift from Prof. James Munro.[63]

HEK293T cell transient transfection

Transient transfections were performed as previously described.[83] Briefly, 2 million HEK293T cells were seeded onto a 10 cm^2 tissue culture dish and allowed to grow for 24 h. For transfection, 10 μg of plasmid were combined with 30 μg polyethyleneimine (PEI) (Fischer Scientific) in 1 mL Opti-MEM media (Gibco) and allowed to incubate for 10 min at room temperature. Plasmid/PEI solution was added dropwise to cell culture and incubated for 24 h at 37 °C. For most experiments, DMEM Media was replaced, and cells allowed to grow for an additional 24 h.

Transfection on SILAC adapted and labeled HEK293T cells were done similarly as normal PEI transfection, except that 1x SILAC DMEM is used instead of Opti-MEM, and no medium change is applied after the transfection.

If virus-like particle (VLP) quantification was required, 1 mL of extracellular media was collected after 48 h. Both transfected and untransfected cells were harvested by trypsin digestion (Gibco) and sedimented at 500*g* for 5 min. Pellets were resuspended in 900 μL 1x PBS and aliquoted into three equal aliquots (corresponding to about 3 million cells per tube), after which all liquid media was aspirated off.

Cell lysis for GCC preparation

Cell lysis for GCC preparation were performed as previously described with a few modifications.[38] Cell pellets were lysed in 66.67 μL lysis buffer per ~1 million cells. In most experiments, 3 million cells were used, and lysed in either 200 μL 1x native buffer (20 mM HEPES, pH 7.8, 20 mM NaCl, 1 mM Mg Acetate) supplemented with 0.85% Octyl β-D-glucopyranoside (OGP) (Chem-Impex) or 200 μL 1x dissociation buffer (20 mM HEPES, pH 7.8, 100 mM NaCl) supplemented with 0.85% OGP. For crosslinking experiments, diothiobis(succinimidyl propoionate) (ThermoFisher Scientific) was added in increasing concentrations directly to lysate. Cells were incubated for 10 min on ice, and nuclei cleared by spinning at 1000*g* for 10 min at 4 °C (except where indicated otherwise in text). The cleared lysate was immediately used for downstream ultracentrifugation assays.

HEK293-CD4-tetHIV-WT and Jurkat-tetHIV-WT cell induction, collection and lysis

For HEK293-CD4-tetHIV-WT cells, 5 million cells were seeded onto 10 cm^2 plates and allowed to adhere overnight. At time of induction, cells were ~60% confluent. Cells were induced with 0.5 μg/ml doxycycline (MP Biomedicals) in complete DMEM

media and incubated at 37 °C for 24 h. Adherent cells were harvested using 5 mM EDTA, washed in 1x PBS, pelleted by centrifugation at 300*g* for 5 min. Cell pellets were then lysed in 1x native lysis supplemented with 0.85% OGP, before snap freezing in liquid nitrogen. For Jurkat-tetHIV-WT cell induction experiments, 5 million cells were grown in 10 cm^2 plates and induced as above in complete RPMI 1640 media. Cells were harvested by centrifugation at 300*g* for 5 min, after washing with 1x PBS. The collected cell pellets were lysed and snap frozen as above.

Electron microscopy

Gag in various genetic backgrounds was transfected into HEK293T cells using PEI as above, and VLPs expressed for 34–72 h. Media was collected from the cells and clarified by centrifugation at 1,000 xg for 10 min prior to purification on a sucrose gradient cushion. VLPs were exchanged into imaging buffer A (50 mM Tris, pH 7.5, 100 mM NaCl, 0.1 mM EDTA, 1 mM MgCl2) and concentrated using 100 kDa MW cutoff Amicon Ultra Centrifugal Filters (Millipore).

Negative stain grids were prepared by applying 7.5 μl of concentrated VLP sample onto 400 mesh copper carbon-coated grid (Electron Microscopy Sciences, CF400-Cu-25) which was treated by negatively glow-discharge (Electron Microscopy Sciences, EMS100) for 2 min. The grids were then blotted, and 75 μl of freshly prepared 2% uranyl formate (Electron Microscopy Sciences) was added 2 min followed by filter paper blotting (Whatman). Grids were imaged using a Philips CM 100 Transmission Electron Microscope (FEI) operated at 80 kV with a tungsten filament and equipped with a Megaview G2 CCD camera (Olympus Soft Imaging Solutions). Images were recorded at a magnification of 46,000×.

Sucrose gradient ultracentrifugation assays

All reported sucrose percentages are based on w/v measurements. Sucrose gradient ultracentrifugation procedures were adapted from Reed *et al.*[38]. Step gradients were manually poured, containing equal-volumes 10, 15, 20, 40, 50, 66 and 80% sucrose (w/v) steps in 1x native buffer. Continuous gradients were created using a BIOCOMP Gradient master 108 and pre-recorded mixing protocols for 10–60% and 10–40% sucrose gradients. All continuous gradients contained 1x native or dissociation buffer as noted in the text. Gradients with samples were placed in a Beckman SW41Ti rotor and sedimented for 100 min at 35,000 rpm (step gradients), 180 min at 35000 rpm (10–60% continuous gradients), or 960 min at 23,000 rpm (10–40% continuous gradients) in an Optima L-90 K ultracentrifuge (Beckman Coulter).

Membrane floatation assay

Membrane floatation assays were performed as previously described,[35] with a few modifications. 10 million HEK293T cells transfected with Gag-isfGFP were resuspended in 200 μL 1x hypotonic buffer (10 mM Tris Acetate, pH 7.4, 50 mM KCl, 100 mM NaCl, 1 mM Mg Acetate). Cells were then lysed thoroughly in a 1 mL Dounce homogenizer. Raw lysate was combined with 1.8 mL 80% sucrose and placed in the bottom of an ultracentrifuge tube. 8 mL of 60% sucrose were layered on top and finally 1 mL of 10% sucrose layered on top of this. Samples were then centrifuged at 100,000*g* for 4 h, aliquoted by hand-fractionation, and probed for Gag signal via fluorescent readout (see below).

SDS-PAGE and dot blot analysis of GCCs

The presence of Gag was detected using either a combined SDS-PAGE/western blotting or a dot blot/western blotting technique. In all cases, fluorescently labeled α-p24 antibodies (Millipore) and low fluorescence PVDF (BioRad) were used. For dot blotting, PVDF was first activated with 100% methanol, then layered on filter paper, rinsed generously with 1x PBS and place in a 96 well dot blot apparatus (Schleicher and Schuell). 50 μL of fractionated samples were diluted in 100 μL dDH2O and loaded onto PVDF through the dot blot apparatus via vacuum. Loaded PVDF membranes were placed in a 1% milk solution for 30 min, washed three times with 1x PBST, and fluorescent signal visualized using a VersaDoc Imager (BioRad). Samples were quantified using Image Studio Lite (Li-Cor Biosciences), and manually corrected for differences in fluorescence excitation field. For absolute quantification, purified Gag (generous gift of the John Elder Lab) was loaded into the dot blot apparatus at defined concentrations as a concentration standard.

Imaging fluorescently labelled Gag and $A_{[260]}$

Relative sfGFP, mRuby, and $A_{[260]}$ signals were quantified using an EnVision 2104 Multilabel Reader (Perkin Elmer).

Extracellular Gag quantification

1 mL of extracellular media from each sample was collected directly before harvesting Gag-producing cells. Samples were spun at 500*g* for 5 min to pellet necrotic or non-adherent cells. To quantify VLP formation, 20 μL of 8.5% OGP were added to 180 μL of media and incubated at room temperature for 10 min. Samples were then blotted onto PVDF membrane and fluorescent Gag signal visualized using a Versa-Doc as described above.

Export efficiency quantification

To quantify the amount of Gag produced per cell, cell lysates were measured for GFP and $A_{[260]}$ signals as described above. Export efficiency was calculated as follows:

$$\left(Gag[ext]/\left(\frac{Gag[int]}{A_{[260]}}\right)\right)$$

where Gag[ext] is the fluorescent signal of extracellular Gag and Gag[int] is the fluorescent signal of intracellular Gag.

Continual monitoring of Gag-GFP and $A_{[260]}$ during gradient collection

GCCs separated on 10–60% native and dissociating sucrose gradients were monitored using a BR-188 Density System (Brandel) attached to an L-4000 UV Detector (Hitachi) to detect $A_{[260]}$, in tandem with a L-3000 Multi Channel Photon Detector (Hitachi) for fluorescent signal detection, and outputs recorded on a D-2500 Chromato-Integrator (Hitachi). UV detector recorder range was set at 2.5 AUFS and Photon Detector sensitivity at 2.0.

GCC purification from sucrose fractions for biochemical analysis

GCC species were prepared after separation on sucrose gradients by pooling similar factions and exchanging sucrose for 1x corresponding buffer using Amicon Ultra 0.5 mL centrifugal filters (Millipore). For RNase treatment of GCC species, 50 units of RNase A (Sigma) were added to each fraction and allowed to incubate at room temperature for 30 min.

Protein production in E. coli

Protein production – plasmids were transformed into BL21(DE3) pLysS competent cells. Single-colonies were inoculated into 1 mL LB containing 100 μg/mL ampicillin (LB-Amp) and grown for ~6 h at 37 °C with shaking. 50 mL LB-Amp cultures were inoculated with 1 mL cultures and grown overnight at 37 °C. 1 L LB-Amp cultures were inoculated with 20 mL of overnight culture and grown at 37 °C to an optical density at 600 nm of ~0.6. At this point, isopropyl-β-D-1-thiogalactopyranoside (IPTG) was added to a final concentration of 0.4 mM and the temperature lowered to 30 °C. Cultures were grown for an additional 3 h before being harvested by centrifugation and stored at –80 °C.

Protein purification from E. coli

Frozen cell pellets (~5 g) were thawed in 30 mL Buffer A (50 mM Tris-HCl pH 8.0, 10 mM β-mercaptoethanol, 1 M NaCl, 1% Tween-20, 10% glycerol, 25 mM imidazole) and lysed by sonication. Cell debris was removed by centrifugation and the resulting supernatant was applied to a 5-mL HisTrap column (GE) and washed with 5 column volumes of Buffer A. Protein was eluted with a 10 column volume gradient to 100% Buffer B (50 mM Tris-HCl pH 8.0, 10 mM β-mercaptoethanol, 1 M NaCl, 1% Tween-20, 10% glycerol, 500 mM imidazole). Fractions containing the protein of interest were frozen and stored at −80 °C until further use.

Purification and fluorescent labeling of ribosomes

HAP1 cell seeded onto a 10 cm^2 plate and grown to ~80% confluency was washed off by pipetting in cold PBS, and pelleted. Pelleted Cells (about 10 million) were lysed in 200 μL of HAP1 buffer (20 mM HEPES, pH 7.9, 10 mM NaCl, 1 mM Mg Acetate, 1.5 mM DTT) supplemented with 0.85% Octyl β-D-glucopyranoside (OGP), protease inhibitor cocktail (Roche) and RNase inhibitor for 10 min on ice and nuclei pelleted by centrifugation at 18,000*g* for 10 min at 4 °C. SNAP-Surface Alexa Fluor 647 (NEB) were added to the cleared lysate at a final concentration of 10 μM. The lysates were incubated at 37 °C for 30 min. The sample was then layered onto a 4 mL sucrose cushion (20 mM HEPES, pH 7.9, 10 mM NaCl, 1 mM Mg Acetate, 1.5 mM DTT, 30% sucrose w/v) and spun at 32,500 rpm for 14 h at 4 °C in an SW 41 Ti rotor (Beckman Coulter). The resulting pellet was resuspended in 500 μL of HAP1 buffer and insoluble material removed by pelleting using centrifugation at 18,000*g* for 10 min.

Methanol-Chloroform precipitation of protein for mass spectrometry

For a given sample volume, 4 volumes of Methanol and 1 volume of Chloroform were added and vortexed thoroughly. 3 volumes of dDH2O was added followed by vortexing and centrifugation at 18,000*g* for 1 min at room temperature. The upper phase was discarded without disturbing the protein-containing interphase. 3 volumes of Methanol were then added and the sample vortexed and centrifuged again. All liquid was carefully removed, and the sample air dried on bench top. The dried samples were then resuspended in MS digestion buffer (50 mM Ammonium bicarbonate, pH 7.8, 8 M Urea).

Nucleic acid purification from sucrose gradients and agarose gel analysis

100 μL of individual sucrose gradient fraction were transferred into a separate 1.7 ml Eppendorf tubes and mixed with 100 μL of Phenol/Chloroform/Isoamyl Alcohol pH 6.7 (Fisher Biotech). The samples were vortexed thoroughly and incubated at 4 °C overnight. Samples were

spun at 18,000*g* for 30 min at 4 °C and RNA-containing aqueous phases mixed with loading dye (NEB) and analyzed using a 2% agarose TAE gel containing ethidium bromide.

Fluorescence imaging

HEK293T cells were grown on poly-L-lysine coated glass coverslips (Corning) and transfected with Gag-isfGFP and mutants as described above. After 24 h, cells were washed well with 1x PBS, and nuclei stained with Hoescht 33342 (Fischer Scientific), and washed twice more with 1x PBS. Cells were then fixed by incubating slides in 4% paraformaldehyde and 1x PBS for 2 min at room temperature. Liquid was aspirated off and replaced with a 1.5% paraformaldehyde in 1x PBS and incubated for an additional 20 min. Cells were then washed thoroughly with 1xPBS and cured onto glass slides using Prolong Gold (Fisher Scientific), sealed with nail polish, and stored at 4 °C until imaged. All images were recorded on an LSM 780 confocal microscope (Zeiss) at the Scripps Research Institute Microscopy core. Gag-isfGFP and Hoescht signals were detected using 488 and 405 nm excitation lasers respectively.

Single-molecule pulldown assays

Quartz slides were cleaned, passivated with polyethylene glycol (PEG; 95% mPEG-SVA, 5% biotin-PEG-SVA; Laysan Bio), and assembled into sample chambers as previously described.[84] The sample chamber was incubated with 100 μg/mL neutravidin for 2 min, washed twice (90 μL injections) with Antibody Binding Buffer (50 mM HEPES pH 7.5, 150 mM NaCl), then incubated with ~20 nM biotinylated α-GFP antibody for 5 min (Rockland antibodies & assays). The concentration of α-GFP antibody required for GCC immobilization was determined using Gag-isfGFP VLPs that had been treated with detergent (data not shown). The sample chamber was washed again with Antibody Binding Buffer followed by Pulldown Buffer (50 mM HEPES pH 7.5, 10 mM NaCl, 1 mM MgCl2). 90 μL of diluted sucrose gradient fraction sample was applied to the chamber and allowed to incubate for 10 min before a final wash with three injections of Pulldown Buffer. The dilution of sucrose gradient fraction samples was done in Pulldown Buffer (100 × dilution for 10S fractions, 10 × dilution for all others). Control experiments using purified sfGFP were performed as described above using ~0.1 nM antiGFP antibody and 1 nM sfGFP. More information about this assay can be found in Aggarwal and Ha.[85] Single-molecule fluorescence movies were acquired with 488 nm excitation on a custom-built prism-type TIRF microscope, described previously,[86] using custom data acquisition software (available at https://cplc.illinois.edu/software/).

Single-molecule fluorescence data analysis

All smTIRF data processing steps were performed with custom Python 3 software written in house. It was found that artificially increasing the image resolution helped to get more accurate spot detection. Briefly, the first 50 frames of each movie were averaged to reduce noise. The 256x512 pixel image was resampled to a 512x1056 pixel area using a 2-dimensional cubic spline interpolation algorithm (SciPy). Spot center coordinates and radii were determined using a Laplacian of Gaussian blob detection algorithm (Scikit-image). The xy-coordinates and radii were then converted back to the original resolution, and aperture photometry was used to extract fluorescence intensities for each frame and each spot. Briefly, pixel intensities within a circular mask centered on each spot with the predetermined radius were summed to determine the total spot intensity. The median intensity of pixels in a circular annulus with radius r + 2 pixels larger than the spot mask was used as a per pixel background estimator for each frame. Background-adjusted intensities were then normalized to a fixed spot area (in pixels). Initial spot intensities were calculated as the median intensity of the first 10 frames for each spot. When required, the optimal number of bins was calculated as $\sqrt{N} + 1$ (where N is the number of data points) and bins spaced equally across the entire data range. For Figure 3(B) and Supplementary Figure 3(A), the optimal bin width was calculated for the ε native fraction (which has the largest data range) and this bin width was applied to all other GCC fractions. For Supplementary Figure 3(B), the bin width was calculated for the α native fraction and applied to all other GCC fractions. For Figure 3(C), spots having an intensity less than $(3\mu + 3\sigma)$ were considered to be in the low oligomerization state.

GCC α spike experiment

GCC α complexes containing stable isotope-labeled arginine and lysine were purified as previously described from SILAC labeled GagisfGFP-expressing HEK293T cells. Purified GCC α was concentrated and added to native lysis buffer and dissociation lysis buffer to make 1x native lysis buffer with α and 1x dissociation lysis buffer with α. Unlabeled Gag-expressing HEK293T cells were lysed with both labeled-GCC-containing buffers as previously mentioned and analyzed using sucrose gradient as previously mentioned. The incorporation of labeled Gag in

cleared cell lysate and individual GCCs were assessed using targeted mass spectrometry.

Pulse labeling experiment

HEK293T cells cultured in the SILAC adaptation medium was transfected with GagisfGFP as previously described. 24 h after the transfection, the medium was changed to the SILAC labeling medium, and the old medium was stored on ice. Then, 2, 4, 6, 8, 10 h after the medium switch. Cells and medium were harvested. All harvested cells were collected by trypsinization, followed by one 1x PBS wash, pelleted by centrifugation, and flash-frozen in liquid nitrogen in aliquots. Medium from each time point was combined with the corresponding old medium from its plate and centrifuged at 1000*g* for 5 min to remove any dead cells. Then VLP was collected from all mediums by sucrose cushion. The pelleted VLP was resuspended in 320 μL of 1x native lysis buffer supplemented with 0.85% OGP.

Sucrose cushion for VLP collection

25 mL Harvested medium was load on top of 5 mL 20% sucrose w/v in 1x native lysis buffer. The cushion was placed in a Beckman SW28 rotor and sedimented for 140 min at 19400 rpm in an Optima L-90K ultracentrifuge (Beckman Coulter).

Mass spectrometry

All samples, sucrose gradient fraction, cell lysate or VLP lysate, were first methanol/chloroform precipitated. The precipitant was solubilized in 50 μL of MS digestion buffer (8 M Urea, 50 mM Ammonium Bicarbonate, pH 7.8), treated with 5 mM DTT at 37 °C for 1 h then 15 mM iodoacetamide at 30 °C for 30 min in darkness. The sample was first digested with 3 μg of Trypsin/LysC mix (Promega) for 3 h at 37 °C, and then 50 mM Ammonium Bicarbonate, pH 7.8 was added to sample to dilute Urea concentration down to 1 M before the sample was further incubated overnight at 37 °C. After adding ACN to 5% and TFA to 0.5%, the sample was desalted using Pierce C-18 column (Thermo Scientific). The eluted peptide was evaporated (speedvac) to dryness.

Peptides were analyzed on a Sciex 5600 + Triple TOF mass spectrometer coupled to an Eksigent nano-LC 400 system. Samples were loaded onto a 350 μm × 0.5 mm ChromXP C18-CL 3 μm 120 Å Trap column. Peptides were resolved using a 60 min 5%–35% acetonitrile gradient run over a 75 μm × 15 cm ChromXP 3C18-CL 3 μm 120 Å analytical column. Each sample was analyzed in an unscheduled targeted acquisition mode using a cycle consisting of 100 ms MS1 followed by multiple successive 150 ms MS2 scans. The collision energy was calculated using Skyline.[87] The targeted method was also constructed through Skyline.

Heavy-isotope label incorporation: Quantification and fitting

The quantification of unlabeled and labeled peptides was done in Skyline and adapted from Chen *et al.*[88]. The abundance of all peptides was calculated as the sum of product ion transitions. The percentage labeling of protein was calculated by ratio the abundance of labeled protein over the sum of the abundance of labeled and unlabeled protein. Lysate pulse-labeling data was fit using the single exponential function:

$$100\left(1 - e^{-kt}\right)$$

where t represents time, and k represents the labeling rate constant.

Pulse labeling of Gag was fit using the following:

$$100\left(1 + ae^{-k\left(1+\frac{1}{a}\right)t} - (1+a)e^{-kt}\right)$$

As above, t is time, k is the labeling rate constant for the corresponding population, and a is the relative abundance of the precursor population and the product population.

Acknowledgments

Funding for this work was provided by the National Institute of General Medical Sciences (NIH U54 GM103368 B.E.T. PI, to J.A.H., R.P., J. R.W., D.P.M.; NIH GM044060 to D.P.M., NIH R01 GM053757 to J.R.W. and J.N.R-G.), the National Institute of Allergy and Infectious Diseases (NIH U54 AI103368 B.E.T. PI, to J.A.H., R.P., J.R.W., D.P.M.; NIH T32 AI007354 to R.P.), National Heart, Lung, and Blood Institute (NIH F30 HL137563 to S.O.), and The Skaggs Institute For Chemical Biology (Y.D.). Further support was made possible with help from the San Diego Center for AIDS Research (SD CFAR), an NIH-funded program (P30 AI036214), which is supported by the following NIH Institutes and Centers: NIAID, NCI, NHLBI, NIA, NICHD, NIDA, NIDCR, NIDDK, NIGMS, NIMH, NIMHD, FIC, and OAR. We would like to thank Dr. Theresa Fassel for valuable help imaging VLPs using EM. All EM and confocal microscopy was performed at The Scripps Research Institute Microscopy Core Facility. We also would like to thank Dr. Karin Musier-Forsyth for critical reading of this manuscript and providing valuable suggestions.

Author contributions

Y.D., J.A.H., R.P., D.P.M., B.E.T. and J.R.W. conceived of the idea and participated in the writing of the paper. Y.D. and J.A.H. performed

gradient ultracentrifugation experiments. Y.D., J.A. H., S.O. and I.C. prepared cell samples. J.A.H., R. P. and R.L. performed single molecule experiments. J.A.H. and S.H. performed cell imaging experiments. Y.D. performed mass spectrometry experiments. Y.D. and J.N.R-G. performed electron microscopy experiments. All authors discussed the results and commented on the paper.

Declaration of Competing Interest

The authors declare that they have no known competing financial interests or personal relationships that could have appeared to influence the work reported in this paper.

Appendix A. Supplementary material

Supplementary data to this article can be found online at https://doi.org/10.1016/j.jmb.2021.166842.

Received 19 October 2020;
Accepted 20 January 2021;
Available online 1 February 2021

Keywords:
HIV-1;
viral assembly;
isotopic pulse labeling;
smTIRF;
sucrose gradient

† Present address: Department of Biochemistry & Cellular and Molecular Biology, University of Tennessee, Knoxville, Knoxville, TN 37996, United States.
‡ These authors contributed equally to this work.
§ Lead Contact.

References

1. Freed, E.O., (2015). HIV-1 assembly, release and maturation. *Nature Rev. Microbiol.*, **13**, 484–496.
2. Aldovini, A., Young, R.A., (1990). Mutations of RNA and protein sequences involved in human immunodeficiency virus type 1 packaging result in production of noninfectious virus. *J. Virol.*, **64**, 1920–1926.
3. Gorelick, R.J., Nigida Jr., S.M., Bess Jr., J.W., Arthur, L.O., Henderson, L.E., Rein, A., (1990). Noninfectious human immunodeficiency virus type 1 mutants deficient in genomic RNA. *J. Virol.*, **64**, 3207–3211.
4. De Guzman, R.N., Wu, Z.R., Stalling, C.C., Pappalardo, L., Borer, P.N., Summers, M.F., (1998). Structure of the HIV-1 nucleocapsid protein bound to the SL3 psi-RNA recognition element. *Science*, **279**, 384–388.
5. Amarasinghe, G.K., De Guzman, R.N., Turner, R.B., Chancellor, K.J., Wu, Z.R., Summers, M.F., (2000). NMR structure of the HIV-1 nucleocapsid protein bound to stem-loop SL2 of the psi-RNA packaging signal. Implications for genome recognition. *J. Mol. Biol.*, **301**, 491–511.
6. Jouvenet, N., Simon, S.M., Bieniasz, P.D., (2009). Imaging the interaction of HIV-1 genomes and Gag during assembly of individual viral particles. *Proc. Natl. Acad. Sci. USA*, **106**, 19114–19119.
7. Kutluay, S.B., Bieniasz, P.D., (2010). Analysis of the initiating events in HIV-1 particle assembly and genome packaging. *PLoS Pathog.*, **6**, e1001200
8. Jouvenet, N., Neil, S.J., Bess, C., Johnson, M.C., Virgen, C.A., Simon, S.M., et al., (2006). Plasma membrane is the site of productive HIV-1 particle assembly. *PLoS Biol.*, **4**, e435
9. Briggs, J.A., Riches, J.D., Glass, B., Bartonova, V., Zanetti, G., Krausslich, H.G., (2009). Structure and assembly of immature HIV. *Proc. Natl. Acad. Sci. USA*, **106**, 11090–11095.
10. Lu, K., Heng, X., Garyu, L., Monti, S., Garcia, E.L., Kharytonchyk, S., et al., (2011). NMR detection of structures in the HIV-1 5'-leader RNA that regulate genome packaging. *Science*, **334**, 242–245.
11. Schur, F.K., Obr, M., Hagen, W.J., Wan, W., Jakobi, A.J., Kirkpatrick, J.M., et al., (2016). An atomic model of HIV-1 capsid-SP1 reveals structures regulating assembly and maturation. *Science*, **353**, 506–508.
12. Wagner, J.M., Zadrozny, K.K., Chrustowicz, J., Purdy, M. D., Yeager, M., Ganser-Pornillos, B.K., et al., (2016). Crystal structure of an HIV assembly and maturation switch. *Elife*, **5**
13. Brigham, B.S., Kitzrow, J.P., Reyes, J.C., Musier-Forsyth, K., Munro, J.B., (2019). Intrinsic conformational dynamics of the HIV-1 genomic RNA 5'UTR. *Proc. Natl. Acad. Sci. USA*, **116**, 10372–10381.
14. Chen, J., Rahman, S.A., Nikolaitchik, O.A., Grunwald, D., Sardo, L., Burdick, R.C., et al., (2016). HIV-1 RNA genome dimerizes on the plasma membrane in the presence of Gag protein. *Proc. Natl. Acad. Sci. USA*, **113**, E201–E208.
15. Dilley, K.A., Nikolaitchik, O.A., Galli, A., Burdick, R.C., Levine, L., Li, K., et al., (2017). Interactions between HIV-1 Gag and Viral RNA genome enhance virion assembly. *J. Virol.*, **91**
16. VerPlank, L., Bouamr, F., LaGrassa, T.J., Agresta, B., Kikonyogo, A., Leis, J., et al., (2001). Tsg101, a homologue of ubiquitin-conjugating (E2) enzymes, binds the L domain in HIV type 1 Pr55(Gag). *Proc. Natl. Acad. Sci. USA*, **98**, 7724–7729.
17. Pornillos, O., Alam, S.L., Davis, D.R., Sundquist, W.I., (2002). Structure of the Tsg101 UEV domain in complex with the PTAP motif of the HIV-1 p6 protein. *Nat Struct Biol.*, **9**, 812–817.
18. Munshi, U.M., Kim, J., Nagashima, K., Hurley, J.H., Freed, E.O., (2007). An Alix fragment potently inhibits HIV-1 budding: characterization of binding to retroviral YPXL late domains. *J. Biol. Chem.*, **282**, 3847–3855.
19. Fisher, R.D., Chung, H.Y., Zhai, Q., Robinson, H., Sundquist, W.I., Hill, C.P., (2007). Structural and biochemical studies of ALIX/AIP1 and its role in retrovirus budding. *Cell*, **128**, 841–852.
20. Tritel, M., Resh, M.D., (2000). Kinetic analysis of human immunodeficiency virus type 1 assembly reveals the presence of sequential intermediates. *J. Virol.*, **74**, 5845–5855.
21. Campbell, S., Fisher, R.J., Towler, E.M., Fox, S., Issaq, H. J., Wolfe, T., et al., (2001). Modulation of HIV-like particle assembly in vitro by inositol phosphates. *Proc. Natl. Acad. Sci. USA*, **98**, 10875–10879.

22. Jouvenet, N., Bieniasz, P.D., Simon, S.M., (2008). Imaging the biogenesis of individual HIV-1 virions in live cells. *Nature*, **454**, 236–240.
23. Tanaka, M., Robinson, B.A., Chutiraka, K., Geary, C.D., Reed, J.C., Lingappa, J.R., (2016). Mutations of conserved residues in the major homology region arrest assembling HIV-1 Gag as a membrane-targeted intermediate containing genomic RNA and cellular proteins. *J. Virol.*, **90**, 1944–1963.
24. Tomasini, M.D., Johnson, D.S., Mincer, J.S., Simon, S.M., (2018). Modeling the dynamics and kinetics of HIV-1 Gag during viral assembly. *PLoS One*, **13**, e0196133
25. Yang, Y., Qu, N., Tan, J., Rushdi, M.N., Krueger, C.J., Chen, A.K., (2018). Roles of Gag-RNA interactions in HIV-1 virus assembly deciphered by single-molecule localization microscopy. *Proc. Natl. Acad. Sci. USA*, **115**, 6721–6726.
26. Bryant, M., Ratner, L., (1990). Myristoylation-dependent replication and assembly of human immunodeficiency virus 1. *Proc. Natl. Acad. Sci. USA*, **87**, 523–527.
27. Campbell, S., Rein, A., (1999). In vitro assembly properties of human immunodeficiency virus type 1 Gag protein lacking the p6 domain. *J. Virol.*, **73**, 2270–2279.
28. Kawada, S., Goto, T., Haraguchi, H., Ono, A., Morikawa, Y., (2008). Dominant negative inhibition of human immunodeficiency virus particle production by the nonmyristoylated form of gag. *J. Virol.*, **82**, 4384–4399.
29. Lingappa, J.R., Hill, R.L., Wong, M.L., Hegde, R.S., (1997). A multistep, ATP-dependent pathway for assembly of human immunodeficiency virus capsids in a cell-free system. *J. Cell Biol.*, **136**, 567–581.
30. Lee, Y.M., Yu, X.F., (1998). Identification and characterization of virus assembly intermediate complexes in HIV-1-infected CD4+ T cells. *Virology*, **243**, 78–93.
31. Provitera, P., Goff, A., Harenberg, A., Bouamr, F., Carter, C., Scarlata, S., (2001). Role of the major homology region in assembly of HIV-1 Gag. *Biochemistry*, **40**, 5565–5572.
32. Zimmerman, C., Klein, K.C., Kiser, P.K., Singh, A.R., Firestein, B.L., Riba, S.C., et al., (2002). Identification of a host protein essential for assembly of immature HIV-1 capsids. *Nature*, **415**, 88–92.
33. Klein, K.C., Reed, J.C., Tanaka, M., Nguyen, V.T., Giri, S., Lingappa, J.R., (2011). HIV Gag-leucine zipper chimeras form ABCE1-containing intermediates and RNase-resistant immature capsids similar to those formed by wild-type HIV-1 Gag. *J. Virol.*, **85**, 7419–7435.
34. Barajas, B.C., Tanaka, M., Robinson, B.A., Phuong, D.J., Chutiraka, K., Reed, J.C., et al., (2018). Identifying the assembly intermediate in which Gag first associates with unspliced HIV-1 RNA suggests a novel model for HIV-1 RNA packaging. *PLoS Pathog.*, **14**, e1006977
35. Robinson, B.A., Reed, J.C., Geary, C.D., Swain, J.V., Lingappa, J.R., (2014). A temporospatial map that defines specific steps at which critical surfaces in the Gag MA and CA domains act during immature HIV-1 capsid assembly in cells. *J. Virol.*, **88**, 5718–5741.
36. Lingappa, J.R., Reed, J.C., Tanaka, M., Chutiraka, K., Robinson, B.A., (2014). How HIV-1 Gag assembles in cells: Putting together pieces of the puzzle. *Virus Res.*, **193**, 89–107.
37. Singh, A.R., Hill, R.L., Lingappa, J.R., (2001). Effect of mutations in Gag on assembly of immature human immunodeficiency virus type 1 capsids in a cell-free system. *Virology*, **279**, 257–270.
38. Reed, J.C., Molter, B., Geary, C.D., McNevin, J., McElrath, J., Giri, S., et al., (2012). HIV-1 Gag co-opts a cellular complex containing DDX6, a helicase that facilitates capsid assembly. *J. Cell Biol.*, **198**, 439–456.
39. Lingappa, J.R., Thielen, B.K., (2009). Assembly of immature HIV-1 capsids using a cell-free system. *Methods Mol. Biol.*, **485**, 185–195.
40. Tokarev, A., Stoneham, C., Lewinski, M.K., Mukim, A., Deshmukh, S., Vollbrecht, T., et al., (2015). Pharmacologic Inhibition of Nedd8 Activation Enzyme Exposes CD4-Induced Epitopes within Env on Cells Expressing HIV-1. *J. Virol.*, **90**, 2486–2502.
41. Lapek Jr., J.D., Lewinski, M.K., Wozniak, J.M., Guatelli, J., Gonzalez, D.J., (2017). Quantitative temporal viromics of an inducible HIV-1 model yields insight to global host targets and phospho-dynamics associated with protein Vpr. *Mol. Cell Proteomics*, **16**, 1447–1461.
42. Reed, J.C., Westergreen, N., Barajas, B.C., Ressler, D.T. B., Phuong, D.J., Swain, J.V., et al., (2018). Formation of RNA granule-derived capsid assembly intermediates appears to be conserved between human immunodeficiency virus type 1 and the nonprimate lentivirus feline immunodeficiency virus. *J. Virol.*, **92**
43. Sette, P., O'Connor, S.K., Yerramilli, V.S., Dussupt, V., Nagashima, K., Chutiraka, K., et al., (2016). HIV-1 nucleocapsid mimics the membrane adaptor syntenin PDZ to gain access to ESCRTs and promote virus budding. *Cell Host Microbe*, **19**, 336–348.
44. Dooher, J.E., Schneider, B.L., Reed, J.C., Lingappa, J.R., (2007). Host ABCE1 is at plasma membrane HIV assembly sites and its dissociation from Gag is linked to subsequent events of virus production. *Traffic*, **8**, 195–211.
45. Lingappa, J.R., Dooher, J.E., Newman, M.A., Kiser, P.K., Klein, K.C., (2006). Basic residues in the nucleocapsid domain of Gag are required for interaction of HIV-1 gag with ABCE1 (HP68), a cellular protein important for HIV-1 capsid assembly. *J. Biol. Chem.*, **281**, 3773–3784.
46. Dooher, J.E., Lingappa, J.R., (2004). Cell-free systems for capsid assembly of primate lentiviruses from three different lineages. *J. Med. Primatol.*, **33**, 272–280.
47. Dooher, J.E., Lingappa, J.R., (2004). Conservation of a stepwise, energy-sensitive pathway involving HP68 for assembly of primate lentivirus capsids in cells. *J. Virol.*, **78**, 1645–1656.
48. Dale, B.M., McNerney, G.P., Hubner, W., Huser, T.R., Chen, B.K., (2011). Tracking and quantitation of fluorescent HIV during cell-to-cell transmission. *Methods*, **53**, 20–26.
49. Hubner, W., Chen, P., Del Portillo, A., Liu, Y., Gordon, R. E., Chen, B.K., (2007). Sequence of human immunodeficiency virus type 1 (HIV-1) Gag localization and oligomerization monitored with live confocal imaging of a replication-competent, fluorescently tagged HIV-1. *J. Virol.*, **81**, 12596–12607.
50. Muller, B., Daecke, J., Fackler, O.T., Dittmar, M.T., Zentgraf, H., Krausslich, H.G., (2004). Construction and characterization of a fluorescently labeled infectious human immunodeficiency virus type 1 derivative. *J. Virol.*, **78**, 10803–10813.
51. Fuchs, G., Petrov, A.N., Marceau, C.D., Popov, L.M., Chen, J., O'Leary, S.E., et al., (2015). Kinetic pathway of 40S ribosomal subunit recruitment to hepatitis C virus internal ribosome entry site. *Proc. Natl. Acad. Sci. USA*, **112**, 319–325.

52. Clark, R.W., (1976). Calculation of s20, w values using ultracentrifuge sedimentation data from linear sucrose gradients, an improved, simplified method. *Biochim. Biophys. Acta*, **428**, 269–274.
53. McEwen, C.R., (1967). Tables for estimating sedimentation through linear concentration gradients of sucrose solution. *Anal. Biochem.*, **20**, 114–149.
54. Ifft, J.B., (1976). Sedimentation equilibrium of proteins in density gradients. *Biophys. Chem.*, **5**, 137–157.
55. Ono, A., Freed, E.O., (1999). Binding of human immunodeficiency virus type 1 Gag to membrane: role of the matrix amino terminus. *J. Virol.*, **73**, 4136–4144.
56. Hogue, I.B., Grover, J.R., Soheilian, F., Nagashima, K., Ono, A., (2011). Gag induces the coalescence of clustered lipid rafts and tetraspanin-enriched microdomains at HIV-1 assembly sites on the plasma membrane. *J. Virol.*, **85**, 9749–9766.
57. von Schwedler, U.K., Stray, K.M., Garrus, J.E., Sundquist, W.I., (2003). Functional surfaces of the human immunodeficiency virus type 1 capsid protein. *J. Virol.*, **77**, 5439–5450.
58. Kong, L.B., An, D., Ackerson, B., Canon, J., Rey, O., Chen, I.S., et al., (1998). Cryoelectron microscopic examination of human immunodeficiency virus type 1 virions with mutations in the cyclophilin A binding loop. *J. Virol.*, **72**, 4403–4407.
59. Webb, J.A., Jones, C.P., Parent, L.J., Rouzina, I., Musier-Forsyth, K., (2013). Distinct binding interactions of HIV-1 Gag to Psi and non-Psi RNAs: implications for viral genomic RNA packaging. *RNA*, **19**, 1078–1088.
60. Floderer, C., Masson, J.B., Boilley, E., Georgeault, S., Merida, P., El Beheiry, M., et al., (2018). Single molecule localisation microscopy reveals how HIV-1 Gag proteins sense membrane virus assembly sites in living host CD4 T cells. *Sci. Rep.*, **8**, 16283.
61. Datta, S.A., Heinrich, F., Raghunandan, S., Krueger, S., Curtis, J.E., Rein, A., et al., (2011). HIV-1 Gag extension: conformational changes require simultaneous interaction with membrane and nucleic acid. *J. Mol. Biol.*, **406**, 205–214.
62. Saad, J.S., Miller, J., Tai, J., Kim, A., Ghanam, R.H., Summers, M.F., (2006). Structural basis for targeting HIV-1 Gag proteins to the plasma membrane for virus assembly. *Proc. Natl. Acad. Sci. USA*, **103**, 11364–11369.
63. Munro, J.B., Nath, A., Farber, M., Datta, S.A., Rein, A., Rhoades, E., et al., (2014). A conformational transition observed in single HIV-1 Gag molecules during in vitro assembly of virus-like particles. *J. Virol.*, **88**, 3577–3585.
64. Keane, S.C., Heng, X., Lu, K., Kharytonchyk, S., Ramakrishnan, V., Carter, G., et al., (2015). RNA structure. Structure of the HIV-1 RNA packaging signal. *Science*, **348**, 917–921.
65. Mekdad, H.E., Boutant, E., Karnib, H., Biedma, M.E., Sharma, K.K., Malytska, I., et al., (2016). Characterization of the interaction between the HIV-1 Gag structural polyprotein and the cellular ribosomal protein L7 and its implication in viral nucleic acid remodeling. *Retrovirology*, **13**, 54.
66. Jager, S., Cimermancic, P., Gulbahce, N., Johnson, J.R., McGovern, K.E., Clarke, S.C., et al., (2011). Global landscape of HIV-human protein complexes. *Nature*, **481**, 365–370.
67. Kutluay, S.B., Zang, T., Blanco-Melo, D., Powell, C., Jannain, D., Errando, M., et al., (2014). Global changes in the RNA binding specificity of HIV-1 gag regulate virion genesis. *Cell*, **159**, 1096–1109.
68. Milev, M.P., Ravichandran, M., Khan, M.F., Schriemer, D. C., Mouland, A.J., (2012). Characterization of staufen1 ribonucleoproteins by mass spectrometry and biochemical analyses reveal the presence of diverse host proteins associated with human immunodeficiency virus type 1. *Front. Microbiol.*, **3**, 367.
69. Le Sage, V., Cinti, A., Valiente-Echeverria, F., Mouland, A. J., (2015). Proteomic analysis of HIV-1 Gag interacting partners using proximity-dependent biotinylation. *Virol. J.*, **12**, 138.
70. Anton, H., Taha, N., Boutant, E., Richert, L., Khatter, H., Klaholz, B., et al., (2015). Investigating the cellular distribution and interactions of HIV-1 nucleocapsid protein by quantitative fluorescence microscopy. *PLoS One*, **10**, e0116921
71. Khatter, H., Myasnikov, A.G., Natchiar, S.K., Klaholz, B.P., (2015). Structure of the human 80S ribosome. *Nature*, **520**, 640–645.
72. Hendrix, J., Baumgartel, V., Schrimpf, W., Ivanchenko, S., Digman, M.A., Gratton, E., et al., (2015). Live-cell observation of cytosolic HIV-1 assembly onset reveals RNA-interacting Gag oligomers. *J. Cell Biol.*, **210**, 629–646.
73. Rao, S., Cinti, A., Temzi, A., Amorim, R., You, J.C., Mouland, A.J., (2018). HIV-1 NC-induced stress granule assembly and translation arrest are inhibited by the dsRNA binding protein Staufen1. *RNA*, **24**, 219–236.
74. Cinti, A., Le Sage, V., Ghanem, M., Mouland, A.J., (2016). HIV-1 Gag blocks selenite-induced stress granule assembly by altering the mRNA cap-binding complex. *mBio*, **7**, e0029.
75. Ono, A., Freed, E.O., (2004). Cell-type-dependent targeting of human immunodeficiency virus type 1 assembly to the plasma membrane and the multivesicular body. *J. Virol.*, **78**, 1552–1563.
76. Chukkapalli, V., Oh, S.J., Ono, A., (2010). Opposing mechanisms involving RNA and lipids regulate HIV-1 Gag membrane binding through the highly basic region of the matrix domain. *Proc. Natl. Acad. Sci. USA*, **107**, 1600–1605.
77. Chukkapalli, V., Inlora, J., Todd, G.C., Ono, A., (2013). Evidence in support of RNA-mediated inhibition of phosphatidylserine-dependent HIV-1 Gag membrane binding in cells. *J. Virol.*, **87**, 7155–7159.
78. Ong, S.E., Blagoev, B., Kratchmarova, I., Kristensen, D.B., Steen, H., Pandey, A., et al., (2002). Stable isotope labeling by amino acids in cell culture, SILAC, as a simple and accurate approach to expression proteomics. *Mol. Cell Proteomics*, **1**, 376–386.
79. Adachi, A., Gendelman, H.E., Koenig, S., Folks, T., Willey, R., Rabson, A., et al., (1986). Production of acquired immunodeficiency syndrome-associated retrovirus in human and nonhuman cells transfected with an infectious molecular clone. *J. Virol.*, **59**, 284–291.
80. Wodrich, H., Bohne, J., Gumz, E., Welker, R., Krausslich, H.G., (2001). A new RNA element located in the coding region of a murine endogenous retrovirus can functionally replace the Rev/Rev-responsive element system in human immunodeficiency virus type 1 Gag expression. *J. Virol.*, **75**, 10670–10682.
81. Gibson, D.G., Young, L., Chuang, R.Y., Venter, J.C., Hutchison 3rd, C.A., Smith, H.O., (2009). Enzymatic

assembly of DNA molecules up to several hundred kilobases. *Nature Methods*, **6**, 343–345.
82. Pedelacq, J.D., Cabantous, S., Tran, T., Terwilliger, T.C., Waldo, G.S., (2006). Engineering and characterization of a superfolder green fluorescent protein. *Nature Biotechnol.*, **24**, 79–88.
83. Longo, P.A., Kavran, J.M., Kim, M.S., Leahy, D.J., (2013). Transient mammalian cell transfection with polyethylenimine (PEI). *Methods Enzymol.*, **529**, 227–240.
84. Lamichhane, R., Solem, A., Black, W., Rueda, D., (2010). Single-molecule FRET of protein-nucleic acid and protein-protein complexes: surface passivation and immobilization. *Methods*, **52**, 192–200.
85. Aggarwal, V., Ha, T., (2014). Single-molecule pull-down (SiMPull) for new-age biochemistry: methodology and biochemical applications of single-molecule pull-down (SiMPull) for probing biomolecular interactions in crude cell extracts. *Bioessays*, **36**, 1109–1119.
86. Berezhna, S.Y., Gill, J.P., Lamichhane, R., Millar, D.P., (2012). Single-molecule Forster resonance energy transfer reveals an innate fidelity checkpoint in DNA polymerase I. *J. Am. Chem. Soc.*, **134**, 11261–11268.
87. MacLean, B., Tomazela, D.M., Shulman, N., Chambers, M., Finney, G.L., Frewen, B., et al., (2010). Skyline: an open source document editor for creating and analyzing targeted proteomics experiments. *Bioinformatics*, **26**, 966–968.
88. Chen, S.S., Sperling, E., Silverman, J.M., Davis, J.H., Williamson, J.R., (2012). Measuring the dynamics of E. coli ribosome biogenesis using pulse-labeling and quantitative mass spectrometry. *Mol. Biosyst.*, **8**, 3325–3334.